(A New Proposal to Jefferson Lab PAC 30) Measurement of neutron spin asymmetry A_1^n in the valence quark region using 8.8 GeV and 6.6 GeV beam energies and Bigbite spectrometer in Hall A

G. Franklin, S. Riordan, D. Seymour
Carnegie Mellon University, Pittsburgh, PA 15213

S. Zhou and X. Li
China Institute of Atomic Energy, Beijing, China

D. Armstrong, T. Averett, M. Finn, K. Grimm, T. Holmstrom, A. Kelleher, V. Sulkovsky
College of William and Mary, Williamsburg, VA 23185

W. Boeglin, P. Markowitz
Florida International University, Miami, FL

J. Annand, D. Ireland, I. Lehmann, D. Protopopescu, G. Rosner(Spokesperson), B. Seitz
University of Glasgow, Glasgow G12 8QQ, Scotland, UK

A. Camsonne, J. P. Chen, E. Chudakov, J. Gomez, R. Feuerbach, J.-O. Hansen,
D. Higinbotham, C. de Jager, J. LeRose, R. Michaels, S. Nanda,
A. Saha, B. Wojtsekhowski (Spokesperson and contact person)
Jefferson Lab, Newport News, VA 23606

W. Bertozzi, S. Gilad, A. Puckett, X. Zheng (Spokesperson) *
Massachusetts Institute of Technology, Cambridge, MA 02139

J. Lictensdatd, E. Piasetzky
Tel Aviv University, Tel Aviv, Israel

S. Choi, H. Kang, B. Lee, Y. Oh, J. Song
Seoul National University, Seoul 151-747, Korea

P. Souder
Syracuse University, Syracuse, NY 13122

A. Lukhanin, Z.-E. Meziani(Spokesperson), B. Sawatzky
Temple University, Philadelphia, PA 19122

S. Sirca
University of Kentucky, Lexington, KY 40506
University of Ljubljana, Slovenia

K. Allada, C. Dutta, W. Korsch, A. Kolarkar
University of Kentucky, Lexington, KY 40506

K. Kumar, K. Paschke
University of Massachusetts, Amherst, MA 01003

H. Lu, X. Yan and Y. Ye
University of Science and Technology of China, Heifei, China

G. Cates (Spokesperson), R. Lindgren, N. Liyanage (Spokesperson), V. Nelyubin, J. Singh
University of Virginia, Charlottesville, VA 22904

K. Egiyan, A. Ketikyan, A. Shahinyan, H. Voskanyan
Yerevan Physics Institute, Yerevan, Armenia

July 7, 2006

*Affiliation starting September 2006: University of Virginia, Charlottesville, VA 22904

Abstract

We propose a precision measurement of the neutron virtual photon asymmetry A_1^n in the Deep Inelastic Scattering region up to x_{Bj}= 0.71 using 8.8 and 6.6 GeV beam energies and the Bigbite spectrometer in Hall A. The proposed measurement will provide the first precision data in the valence quark region above x_{Bj}= 0.6 and therefore test various predictions including those from the relativistic constituent quark model and perturbative QCD. Since the predictions from pQCD are quite sensitive to the manner in which quark orbital angular momentum (OAM) is handled, this experiment will provide considerable insight into the evolving picture of the role that quark OAM plays in the nucleon wavefunction. Also, if our proposed data on A_1^n are taken together with similar data on A_1^p it will be possible to perform a flavor decomposition of the polarization of the parton distribution functions. Finally, since this experiment plans to use existing equipment in Hall A, it can run soon after 8.8 GeV beam is available in Hall A as a commissioning experiment, and will establish the Bigbite spectrometer as an invaluable device for studying intermediate to high luminosity physics in Hall A after the 12 GeV upgrade.

1 Introduction

We are proposing a precision measurement of the virtual photon asymmetry A_1^n of the neutron in the Deep Inelastic Scattering (DIS) region ($W^2 > 4$ GeV^2) using the Hall A polarized ^{3}He target and the Hall A Bigbite spectrometer up to $x_{Bj} \approx 0.71$. Within the quark parton model, the asymmetry A_1 provides well defined information about the spin carried by the quarks. At high values of x_{Bj}, where the sea quarks make a minimal contribution, knowledge of A_1 for the neutron and proton taken together translates into a flavor separated measurement of the polarization of the parton distribution functions. Perhaps even more interesting, however, is the fact that in the high x_{Bj} region A_1 can be calculated using perturbative QCD (pQCD). These calculations are quite sensitive to the manner in which quark orbital angular momentum (OAM) is handled. A measurement of A_1 thus gives us insight into the important question of the role of quark OAM in the nucleon wave function.

Both pQCD and the relativistic constituent quark model (RCQM) predict that as $x_{Bj} \to 1$ both A_1^p and A_1^n asymptotically approach unity. Until quite recently, however, the measured values for A_1^n had either been negative or consistent with zero. A recent measurement of A_1^n, however, provided clear evidence of A_1^n becoming positive above roughly x_{Bj}=0.5 [1]. The value measured was consistent with expectations from the RQPM, but not with pQCD calculations in which "hadron helicity conservation" or HHC is assumed. The assumption of HHC essentially precludes a contribution to A_1^n from quark OAM. The apparent disagreement between the measurement of ref. [1] and the earlier pQCD calculations can be interpreted as evidence for the importance of quark OAM. Indeed, more recent pQCD calculations that retained coefficients with logarithmic dependences are more consistent with observation. These more recent calculations explicitly include effects that correspond to non-zero quark OAM.

The figure clearly shows that the current experimental accuracy of A_1^n in the high x_{Bj} region is insufficient. Furthermore, most of the theoretical predictions for A_1^n have been made in the Bjorken limit. The naive expectation has been that since A_1 is roughly the ratio between the structure functions g_1 and F_1, both of which show similar scaling violations due to gluon radiation, A_1 would show little or no Q^2 dependence. However, we have no understanding of the Q^2 dependence of A_1 arising due to quark orbital angular momentum effects and higher twist effects. Therefore if we are to understand the behavior of A_1^n approaching the Bjorken limit, we need to measure it not only at a single set of Q^2 values, but over a range of Q^2 values. The large acceptance of the Bigbite spectrometer combined with the high polarized luminosity of the hall A polarized ^{3}He target allows us to measure A_1^n over a range of Q^2 values in the high x_{Bj} region.

Due to the large momentum acceptance of the Bigbite spectrometer, the proposed experiment also provides us with two "free" datasets in the resonance region covering the high x_{Bj} and high Q^2 region. Altogether, the proposed measurement provides a comprehensive mapping of A_1^n in the DIS and resonance regions up to $x_{Bj} \approx 0.83$ and $Q^2 \approx 10$ GeV^2.

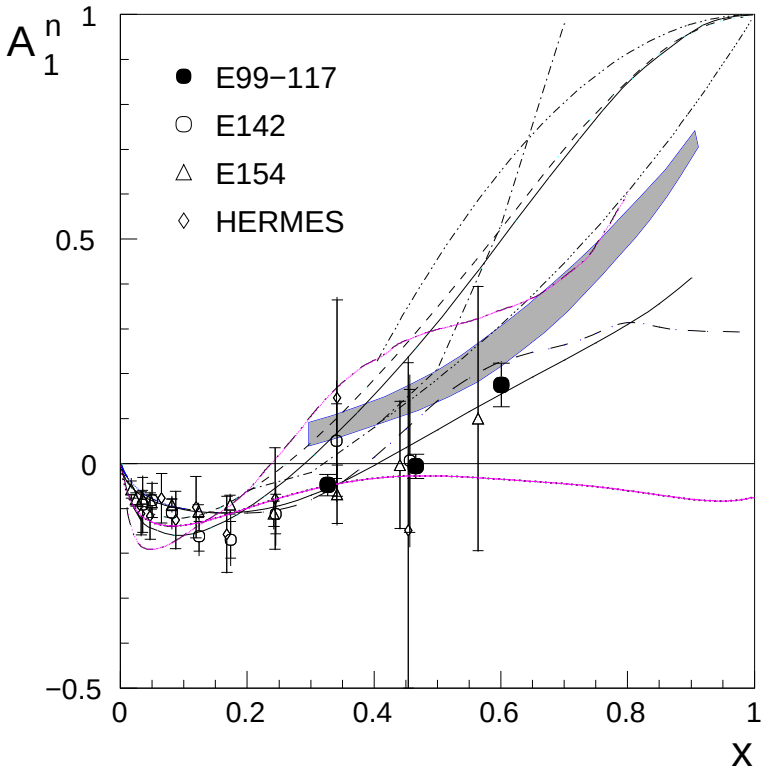

Figure 1: A sample of Previous A_1^n results [1, 2, 3, 4] compared to theoretical predictions: predictions of A_1^n from SU(6) symmetry (x_{Bj} axis at zero) [5], constituent quark model (shaded band) [6], statistical model at $Q^2 = 4$ (GeV/c)^2 (long-dashed) [7], quark-hadron duality using two different SU(6) breaking mechanisms (dash-dot-dotted and dash-dot-dot-dotted), and non-meson cloudy bag model (dash-dotted) [8]; predictions of g_1^n/F_1^n from pQCD HHC based BBS parameterization at $Q^2 = 4$ (GeV/c)^2 (higher solid) [61] and LSS(BBS) parameterization at $Q^2 = 4$ (GeV/c)^2 (dashed) [62], LSS 2001 NLO polarized parton densities at $Q^2 = 5$ (GeV/c)^2 (lower solid) [11] and chiral soliton models [12] at $Q^2 = 3$ (GeV/c)^2 (long dash-dotted) and [13] at $Q^2 = 4.8$ (GeV/c)^2 (dotted).

2 Collaboration contributions to 12 GeV baseline equipment

There are four items listed under Hall A 12 GeV baseline equipment:

- arc energy measurement system,
- the Compton polarimeter,
- the Moller polarimeter,
- the HRS readout electronics.

This collaboration **intends** to make major contributions to the **readout electronics upgrade of HRS**. In this project we plan to contribute in development of the software and hardware as well as in commissioning of electronics in beam. The members of the University of Virginia group are already involved in the upgrade of the **Compton polarimeter**. This involvement **will continue into upgrading and commissioning** of the Compton polarimeter for the high energy beam. As proposed this experiment will be a commissioning experiment for Hall A, so the collaboration **intends** to made major contributions in design and commissioning of the equipment for **arc energy measurement system**. The spokespeople of this experiment include members of three strong university research groups that have played a major role in the Hall A physics program. From the inception of Hall A these spokespeople have made significant contributions to the base equipment in Hall A. These include important contributions in the instrumentation and commissioning of the Hall A high resolution spectrometer pair, construction and support of the Hall A polarized ^{3}He target and instrumentation and commissioning of the Bigbite spectrometer.

The following is a list of personnel (and FTE-years) from the institutions committed to the 12 GeV Baseline equipment:

- The university of Virginia group has three faculty members, one post-doc and several graduate students committed to this project. The major source of research funding for this group is DOE. Intended contribution is 2 FTE-years.
- Temple University group has one faculty member, a post-doctoral associate, a research associate, and several graduate student. The major source of research funding for this group is DOE. Intended contribution is 1 FTE-years.
- University of Glasgow group has three faculty members, two research scientists and one post-doc committed to this experiment. The major source of research funding for this group is the UK Engineering and Physical Sciences Research Council, EPSRC. Intended contribution is 2 FTE-years.

We would like also to point out that with this proposal, our collaboration is committing itself to maintain and improve the Hall A polarized ^{3}He target and the Bigbite spectrometer. Although Hall A polarized ^{3}He target is not in the list of 12 GeV Baseline equipment, it is central to many important experiments planed with the 12 GeV beam and its peak performance will be crucial to the 12 GeV physics program in both Hall A and Hall C. As we have shown in this proposal, Bigbite will be a valuable device for moderate luminosity

experiments with the upgraded CEBAF beam. Therefore the successful commissioning of Bigbite for the high energy beam with this proposed experiment has the potential of providing high importance result as soon as high energy beam available from accelerator, significantly reducing the Beam time pressure on Hall C, and increasing the physics output of upgraded Jefferson lab.

3 Physics Motivation

3.1 Background

When Bjorken first published his famous sum rule in 1966 [14], he referred to it as a "worthless equation", assuming that it dealt with quantities that were impractical to measure. By the late 1970's, however, the field of the spin structure of the nucleon was firmly established. Interest in the field soared when the EMC published their result on the integral of the proton polarized structure function g_1^p which indicated that the total spin carried by quarks was very small, $\approx (12 \pm 17)\%$ [15], a paper that at the time of this writing has 1293 citations, making it the 99th most cited paper on Spires. The EMC result was in sharp contrast to the expectations of SU(6) in which 100% of the spin is carried by the quarks, or the relativistic constituent quark model in which roughly 75% of the proton spin is expected to arise from the quarks.

The various contributions to the spin of the nucleon can be summarized by a simple equation:

$$S_z^N = \tfrac{1}{2}\Delta\Sigma + L_z^q + \Delta G + L_z^g = \tfrac{1}{2} \ , \tag{1}$$

where S_z^N is the nucleon spin, $\Delta\Sigma$ is the fraction of the nucleon spin due to the spin of the quarks, and L_z^q, ΔG, and L_z^g are the contribution to the nucleon spin due to the orbital angular momentum (OAM) of the quarks, the spin of the gluons, and the OAM of the gluons respectively. Within the $\overline{\text{MS}}$ renormalization scheme, it is generally accepted that about $(20-30)\%$ of the nucleon spin is carried by the spin of the quarks. While the existing data on ΔG are still quite limited, it now appears likely that ΔG is relatively small, in contrast to some early speculations. Thus, by process of elimination if nothing else, it appears increasingly likely (although not certain!) that OAM plays an important role in the static spin properties of the nucleon.

When the discovery was made at JLab that G_E^p/G_M^p decreases almost linearly with Q^2, it quickly became apparent that the OAM of the quarks plays an important role in the nucleon wave function. As already mentioned in the introduction to this proposal, further evidence for the importance of quark OAM came from the disagreement of the measured value for A_1^n at $x = 0.6$ measured by Zheng *et al.*[1] with pQCD predictions based on HHC. There are now, in fact, quite a few results from JLab from which one can draw similar conclusions.

3.2 Definitions

The virtual photon asymmetry A_1 is defined as

$$A_1(x, Q^2) \equiv \frac{\sigma_{1/2} - \sigma_{3/2}}{\sigma_{1/2} + \sigma_{3/2}}$$

where $\sigma_{1/2(3/2)}$ is the nucleon's photo-absorption cross section with total helicity of the $\gamma^* - N$ system being 1/2(3/2). A_1 can be related to the unpolarized and the polarized structure functions F_1 and g_1 as

$$A_1(x, Q^2) = \frac{g_1(x, Q^2) - \gamma^2 g_2(x, Q^2)}{F_1(x, Q^2)} \tag{2}$$

where $\gamma^2 \equiv \frac{Q^2}{\nu^2} = \frac{(2Mx)^2}{Q^2}$ and at large Q^2 one has $A_1 \approx g_1/F_1$. The structure functions F_1 and g_1 have explicit implications in the quark-parton model:

$$F_1(x,Q^2) = \frac{1}{2}\sum_i e_i^2 q_i(x,Q^2) \quad \text{and} \quad g_1(x,Q^2) = \frac{1}{2}\sum_i e_i^2 \Delta q_i(x,Q^2) \ , \tag{3}$$

where $q_i(x,Q^2) = q_i^{\uparrow}(x,Q^2) + q_i^{\downarrow}(x,Q^2)$ and $\Delta q_i(x,Q^2) = q_i^{\uparrow}(x,Q^2) - q_i^{\downarrow}(x,Q^2)$ are the unpolarized and the polarized parton distribution functions, respectively.

3.3 SU(6) Non-Relativistic Constituent Quark Model

In the simplest non-relativistic constituent quark model (CQM) [16], the nucleon is made of three constituent quarks and the nucleon spin is due entirely to the quark spins. Assuming SU(6) symmetry, the wavefunction of a neutron polarized in the $+z$ direction then has the form [5]:

$$\begin{aligned} |n\uparrow\rangle = & \frac{1}{\sqrt{2}}\left|d^{\uparrow}(du)_{000}\right\rangle + \frac{1}{\sqrt{18}}\left|d^{\uparrow}(du)_{110}\right\rangle \\ & -\frac{1}{3}\left|d^{\downarrow}(du)_{111}\right\rangle - \frac{1}{3}\left|u^{\uparrow}(dd)_{110}\right\rangle + \frac{\sqrt{2}}{3}\left|u^{\downarrow}(dd)_{111}\right\rangle , \end{aligned} \tag{4}$$

where the two spectator quarks form a "diquark" state and the three subscripts are the diquark's total isospin, total spin (S) and the spin projection along the $+z$ direction (S_z). For the case of a proton one needs to exchange the u and d quarks in Eq. (4). In the limit where SU(6) symmetry is exact, both diquark spin states with $S = 1$ and $S = 0$ contribute equally to the observables of interest, leading to the predictions

$$A_1^p = 5/9 \ , A_1^n = 0 \ , \Delta u/u = 2/3, \quad \text{and } \Delta d/d = -1/3. \tag{5}$$

In the case of DIS, exact SU(6) symmetry implies the same shape for the valence quark distributions, *i.e.* $u(x) = 2d(x)$. Assuming that $R(x,Q^2) \equiv \sigma_L/\sigma_T$ is the same for the neutron and the proton, one can write the ratio of neutron and proton F_2 structure functions as

$$R^{np} \equiv \frac{F_2^n}{F_2^p} = \frac{u(x) + 4d(x)}{4u(x) + d(x)} \ . \tag{6}$$

Applying $u(x) = 2d(x)$ gives $R^{np} = 2/3$. However, data on the R^{np} ratio from SLAC [17], CERN [18, 19, 20] and Fermilab [21] disagree with this SU(6) prediction. The data show that $R^{np}(x_{Bj})$ has almost linear dependance on x_{Bj} starting with $R^{np}|_{x\to 0} \approx 1$ and dropping to below 1/2 as x_{Bj} approaches 1. In addition, $A_1^p(x)$ is small at low x_{Bj} [22, 23, 24]. The fact that $R^{np}|_{x\to 0} \approx 1$ may be explained by the dominance of sea quarks in the low x_{Bj} region and the fact that $A_1^p|_{x\to 0} \approx 0$ could be explained by the polarization of the sea quarks being quite small. At large x_{Bj}, however, there are few sea quarks and the deviation from SU(6) prediction indicates a problem with the wavefunction described by Eq. (4). In fact, SU(6) symmetry is known to be broken [25] and the details of possible SU(6)-breaking mechanisms is an important issue in hadronic physics.

3.4 SU(6) Breaking and Hyperfine Perturbed Relativistic CQM

A possible explanation for the SU(6) symmetry breaking is the one-gluon exchange interaction which dominates the quark-quark interaction at short-distances. This interaction has been used to explain the behavior of R^{np} as $x \to 1$ and the $\approx$ 300-MeV mass shift between the nucleon and the $\Delta(1232)$ [25]. It can be described by an interaction term proportional to $\vec{S}_i \cdot \vec{S}_j \; \delta^3(\vec{r}_{ij})$, with $\vec{S}_i$ the spin of the ith quark, and hence is also called the hyperfine interaction, or chromomagnetic interaction among the quarks [26]. The effect of this perturbation on the wavefunction is to lower the energy of the $S = 0$ diquark state, causing the first term of Eq. (4), $|d \uparrow (ud)_{000}\rangle$ (for the neutron), to become more stable and to dominate the high energy tail of the quark momentum distribution that is probed as $x \to 1$. Since the struck quark in this term has its spin parallel to that of the nucleon, the dominance of this term as $x \to 1$ implies $(\Delta d/d)^{\mathrm{n}} \to 1$ and $(\Delta u/u)^{\mathrm{n}} \to -1/3$ for the neutron, while for the proton one has

$$\Delta u/u \to 1 \text{ and } \Delta d/d \to -1/3 \;\; \text{ as } x \to 1 \; . \tag{7}$$

One also obtains $R^{np} \to 1/4$ as $x \to 1$, which could explain the deviation of $R^{np}(x)$ data from the SU(6) prediction. Based on the same mechanism, one can make the following predictions:

$$A_1^p \to 1 \text{ and } A_1^n \to 1 \;\; \text{ as } x \to 1 \; . \tag{8}$$

The hyperfine interaction is often used to break SU(6) symmetry in the relativistic CQM (RCQM). In this model, the constituent quarks have non-zero OAM which carry $\approx 25\%$ of the nucleon spin [27]. The use of the RCQM to predict the large $x_{_{Bj}}$ behavior of the nucleon structure functions is justified because of valence quark dominance at large $x_{_{Bj}}$. That is, in the large $x_{_{Bj}}$ region almost all quantum numbers, momentum and the spin of the nucleon are carried by the three valence quarks which can therefore be identified as constituent quarks. Isgur has shown that despite various differences, most hyperfine-perturbed RCQM predictions of A_1^n in the large $x_{_{Bj}}$ region, when appropriately constrained, fall within a reasonably narrow and well defined band [6]. Even at $x = 0.6$, which is well below unity, our previously measured value for A_1^n is in reasonable agreement with Isgur's prediction.

3.5 Perturbative QCD and Hadron Helicity Conservation in DIS

In the early 1970's, in one of the first applications of perturbative QCD (pQCD), it was noted that as $x \to 1$, the scattering is from a high-energy quark and thus the process can be treated perturbatively [49]. Furthermore, when the quark OAM is assumed to be zero, the conservation of total angular momentum requires that a quark carrying nearly all the momentum of the nucleon (*i.e.* $x \to 1$) must have the same helicity as the nucleon. This mechanism is called hadron helicity conservation (HHC), and is sometimes referred to as leading-order pQCD. In this picture, quark-gluon interactions cause only the $S = 1$, $S_z = 1$ diquark spin projection component rather than the full $S = 1$ diquark system to be

suppressed as $x \to 1$, which gives

$$\Delta u/u \to 1 \text{ and } \Delta d/d \to 1 \text{ as } x \to 1 \; ; \tag{9}$$

$$R^{np} \to \frac{3}{7}, \; A_1^p \to 1 \text{ and } A_1^n \to 1 \text{ as } x \to 1 \; . \tag{10}$$

This is one of the few places where pQCD can make an absolute prediction for the x_{Bj}-dependence of the structure functions or their ratios. However, how low in x_{Bj} and Q^2 this picture works is uncertain. HHC has been used as a constraint in a model to fit data on the first moment of the proton g_1^p, giving the BBS parameterization [61]. The Q^2 evolution was not included in this calculation. Later in the LSS(BBS) parameterization [62], both proton and neutron A_1 data were fitted directly and the Q^2 evolution was carefully treated. Predictions for A_1^n using both BBS and LSS(BBS) parameterizations are shown in figure 1, and are seen to be inconsistent with our previous data point at $x = 0.6$[1].

HHC is based on the assumption that the quark OAM is zero. However, as mentioned earlier, most explanations of the recent experimental data on G_E^p/G_M^p involve calculations in which quark OAM plays an important role[57, 58, 59, 60]. Studies of single-spin asymmetries also appear to require significant quark OAM to be understood. In addition to the recent measurement of A_1^n, there are other experiments at JLab that appear to signal a breakdown of HHC including data on the tensor polarization in elastic $e -^2$H scattering[52] and neutral pion photoproduction[53]. The fact that the measured value of A_1^n at $x = 0.6$ disagrees with HHC constrained pQCD calculations is probably an indication that quark OAM plays an important role in QCD dynamics at $x = 0.6$. Improving our understanding of A_1^n at high x_{Bj}will allow detailed comparison with pQCD calculations, and may well lead to a better understanding of the limits of HHC and the role of quark OAM.

3.6 Other Predictions

There are many other theoritical predictions for A_1^n including those from chiral soliton models [12, 13], next-to-leading order (NLO) QCD parametrizations [11], bag model [8] and quark-hadron duality [64].

3.7 About the Q^2-Dependence of A_1

In this subsection we review briefly several points concerning the Q^2 dependence of A_1^n. While the Q^2 dependence of A_1^n can legitimately be expected to be fairly weak, it is the case that the precise magnitude of the dependence has not yet been determined, particularly in the high-$x_{Bj}$and relatively low-Q^2 kinematic region in which we are interested. As our study of A_1^n goes beyond mere exploration, it is critical that the contributions to the Q^2 dependence of A_1^n be better understood. Luckily this can be done without performing an exhaustive mapping over both $x_{Bj}$and Q^2. By considering two or three values of Q^2 at a single value of x_{Bj}, it is possible to characterize various effects well enough that we can constrain the degree to which Q^2 dependence will influence the interpretation of our results.

From Eq.(2) one can deduce that $A_1 \approx g_1/F_1$ at large Q^2. One can then naively expect that the Q^2-evolution of g_1 and F_1 follow the same rule in the framework of perturbative

QCD and cancel exactly in their ratio, hence A_1 becomes independent of Q^2. Unfortunately this is not true even if one ignored the obvious $\gamma^2 g_2$ term (which cannot be neglected in the kinematic region achievable at JLab): Only the leading-order and the next-to-leading-order Q^2-evolution of g_1 and F_1 follow the same rule, while their higher orders ($\geq N^2$LO) and higher twist contributions are different. Therefore, although there is some evidence from data that $A_1(x, Q^2)$ is almost independent of Q^2 and it has almost become a tradition in experimental practice to ignore it, there is no justification for believing A_1 to be exactly constant [72]. The experiment proposed here will likely be used for fairly precise flavor-separated determinations of the polarizations of the parton distribution functions, comparison with pQCD calculations, and comparison with lattice calculations. The potentially far-reaching *qualitative* conclusions that will come out of our proposed experiment may well depend critically on our ability to *quantitatively* understand Q^2 dependence and constrain the degree to which it affects our results.

Typically, one can write for $g_1(x, Q^2)$ [71]:

$$g_1(x, Q^2) \;=\; g_1(x, Q^2)_{LT} + g_1(x, Q^2)_{HT} \tag{11}$$

where "LT" denotes the leading twist ($\tau = 2$) contribution to g_1, while "HT" denotes contributions to g_1 arising from QCD operators of higher twist, namely $\tau \geq 3$. The LT contribution can be further written as

$$g_1(x, Q^2)_{LT} \;=\; g_1(x, Q^2)_{pQCD} + h^{TMC}(x, Q^2)/Q^2 + \mathcal{O}(M^4/Q^4) \tag{12}$$

where $g_1(x, Q^2)_{pQCD}$ is the well known (logarithmic in Q^2) pQCD contribution and $h^{TMC}(x, Q^2)$ are the calculable kinematic target mass corrections, which effectively could belong to the LT term. The HT contribution can be written as

$$g_1(x, Q^2)_{HT} \;=\; h(x, Q^2)/Q^2 + \mathcal{O}(\Lambda^4/Q^4) \tag{13}$$

where $h(x, Q^2)$ are the dynamical higher twist ($\tau = 3$ and $\tau = 4$) corrections to g_1. The dynamical HT are related to multi-parton correlations in the nucleon, are non-perturbative and cannot be calculated without using models. Similar descriptions as Eq.(11-13) also work for $F_1(x, Q^2)$. Among all contributions, only the LO and NLO terms of $g_1(x, Q^2)_{pQCD}$ and $F_1(x, Q^2)_{pQCD}$ have the same Q^2-dependences.

In Ref. [71] a formalism was presented to extract the higher-twist contribution to g_1 from data:

$$\left[\frac{g_1(x, Q^2)}{F_1(x, Q^2)}\right]_{exp} \;=\; \frac{g_1(x, Q^2)_{LT} + h(x)/Q^2}{F_1(x, Q^2)_{exp}} \;. \tag{14}$$

where $F_1(x, Q^2)$ is replaced by its expression in terms of the usually extracted from unpolarized DIS experiments F_2 and R. Eq. 14 provides a model-independent way to extract the HT term from data. Results for $h^{g1}(x)$ for both the proton and the neutron are presented in Ref. [71]. However $h^{n,g_1}(x)$ is found to be consistent with zero above $x = 0.2$.

As $x \to 1$, it is well known that higher twist effects should become more important. What is not known is the precise manner in which this happens. By measuring A_1^n at several values of Q^2 it should be possible to quantify or at least constrain these effects.

3.8 Summary of motivation for the proposed experiment

The spin asymmetry A_1 provides several types of insight into the wave function of the nucleon. Within the quark parton model, it provides a direct measurement of the polarization of the parton distribution functions in the valence region. It is also one of the rare quantities describing nucleon structure that is calculable within the framework of pQCD. As such it provides a valuable opportunity to compare theory with experiment, helping us refine our understanding.

Prior to JLab, achieving good statistical accuracy on A_1 was largely impractical at high values of x_{Bj}. This changed with E99-117 in which A_1^n was measured up to a value of $x = 0.6$. While still limited to a moderate value of x_{Bj}, E99-117 was the first experiment to observe A_1^n to become definitively positive. This by itself is an extremely important result, as a failure to become positive would signal profound confusion regarding the nucleon wave function. Furthermore, as discussed above, the point at $x = 0.6$ was consistent with the RCQM, and inconsistent with early pQCD calculations in which HHC was assumed. Taken within the broader context of the various other experiments at JLab that appear to see a breakdown of HHC or other evidence indicating the importance of quark OAM, this is an extremely interesting result.

Using BigBite's large acceptance and the higher beam energies that will be available after the upgrade, we can greatly improve our knowledge of A_1^n. Despite the rapid drop-off in event rate, we demonstrate in this proposal that we can push the range in x_{Bj} over which A_1^n is known from $x_{Bj} = 0.6$ to $x_{Bj} = 0.71$. While naively this may seem like a modest improvement, the expected value of A_1^n, based on the trend observed during E99-117, would be nearly double what it is at $x_{Bj} = 0.6$. Furthermore, the statistical accuracy with which A_1^n will be known at values of x_{Bj} less than 0.71 will be improved by more than a factor of two. In short, the data will begin to seriously constrain theory, thus shedding considerable light on a host of issues ranging from quark OAM to higher-twist effects. The large acceptance of BigBite will also make it possible to begin to study the Q^2 dependence of A_1^n, something that is particularly important when studying high-x_{Bj} physics.

4 The Measurement

We are proposing to use 8.8 GeV and 6.6 GeV longitudinally polarized ($P_e = 0.8$) CEBAF electron beam and the Hall A polarized ^{3}He target. Bigbite spectrometer, located at 30.0° will be used to detect scattered electrons in the range of 1.6 GeV to 3.3 GeV. With the target polarization direction set parallel and perpendicular to the electron beam, the experiment will measure the parallel asymmetry $A_{\parallel}^{^3He}$ and the perpendicular asymmetry $A_{\perp}^{^3He}$. One magnetic field setting of the Bigbite spectrometer with, B= 1.2 Tesla, covers the entire kinematic range of $0.20 \leq x \leq 0.71$ of this proposal. The beam helicity will be reversed at a rate of 30 Hz.

The Hall A left HRS spectrometer, at $-30.0°$ will be used to measure the unpolarized cross section $\sigma_0^{^3He}$ for each proposed bin with high precision. The asymmetry data from HRS, while at a lower statistical precision than the data from Bigbite, will provide an important cross check of every aspect of the data accumulated on Bigbite. The left HRS momentum will be stepped across to cover the kinematic range $0.20 \leq x \leq 0.71$ to measure the absolute cross section as a function of x_{Bj}.

A beam current of 10 μA combined with a target density of 2.5×10^{20} atoms/cm^3 provides an $e - \vec{n}$ luminosity of 5 $\times10^{35}$ cm^{-2}s^{-1} over a 30 cm of target length.

4.1 The Polarized Beam

In this proposal we are assuming an 80% beam polarization with a $10\mu A$ current. The polarization of the beam will be measured with the Hall A Moller and Compton polarimeters.

4.2 The Green Compton Polarimetry

The electron beam polarization can be measured in Hall A using the Compton polarimetry: Because the asymmetry of Compton scattering can be calculated exactly in Quantum Electro-Dynamics (QED), the electron beam polarization can be extracted from cross section asymmetry of scattering between the electron beam and a high power laser. The current Compton Polarimetry in Hall A utilizes a Fabry-Perot cavity operating at 1064 nm (IR) laser with about 1.5 kW intra-cavity power. Both scattered electrons and photons are detected and the beam polarization is extracted from the measured asymmetry of either electron-only events or electron-photon coincidence events. The figure of merit (FOM, $\sigma\langle A\rangle^2$) is proportional to $k^2 \times E^2$ with k the photon energy and E the electron beam energy. The present Compton provides a systematic uncertainty of about 3% for a 4 GeV beam.

For the next a few years there are a few experiments approved to run in Hall A which require higher precision. To meet the requirement of these experiments, an upgrade is being planned [28]: The existing Fabry-Perot cavity will be replaced by a 532 nm (green) cavity with twice the power, resulting in a four-fold enhancement of the FOM of the Compton polarimeter. Associated improvements to the electron detector, the photon calorimeter, and data acquisition method are also required. These upgrades are expected to complete in the next couple of years and are crucial for both the upcoming experiments at 6 GeV and future experiments at the 12 GeV Upgrade. For an 11 GeV beam, the magnetic chicane needs

to be upgraded as well and it will be likely to achieve a 0.5% absolute accuracy of beam polarization measurement after the upgrade is completed.

One of the spokespersons of this proposal is already heavily involved in the Green Compton Upgrade which is on-going in the Green Compton Polarimetry Lab in the ARC building of Jefferson Lab. We expect to continue this effort and make significant contributions to the Green Compton development and commissioning at both 6 and 12 GeV.

4.3 The polarized ^{3}He target

The polarized ^{3}He target at JLab is based on optical pumping of a vapor of alkali atoms and subsequent spin exchange between the polarized atoms and the ^{3}He nuclei.

Figure 2: Typical layout of a polarized ^{3}He target. Note that for simplicity, only one of the three sets of orthogonal Helmholtz coils shown.

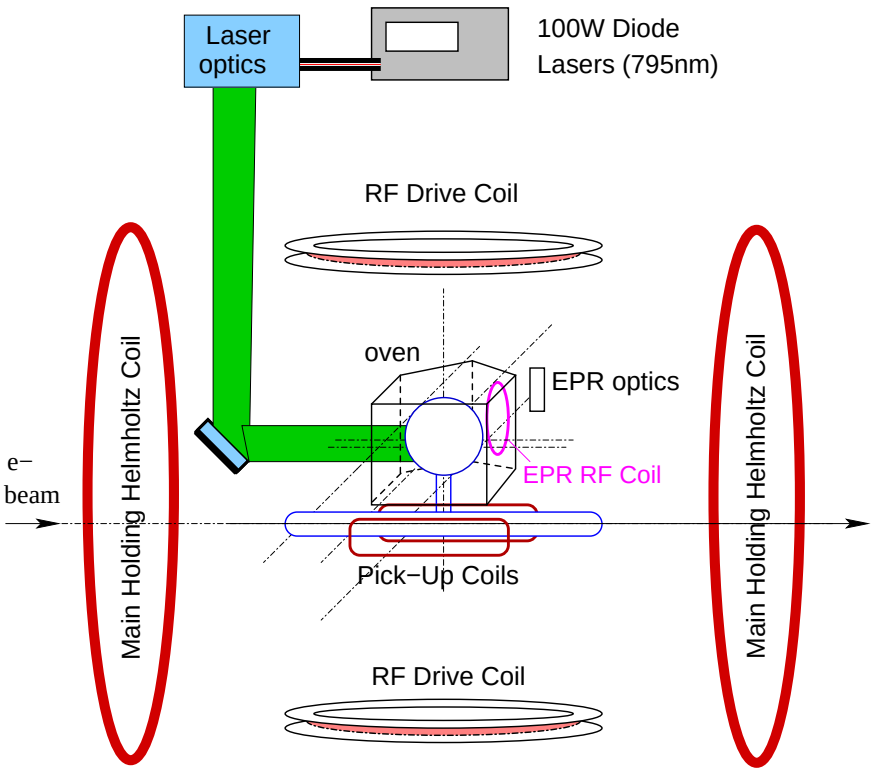

Figure 2 shows the basic layout of the polarized ^{3}He target which currently exists for research in Hall A [29]. The target holding field is provided by two sets of Helmholtz coils oriented normal to each other, hence the target spin direction can be aligned either parallel or perpendicular to the electron beam. Fig. 3 shows a picture of a standard 40 cm long cell. The cells for these experiments consist of a two chamber design. The upper spherical chamber contains the alkali vapor while the lower chamber is used for electron scattering from the polarized ^{3}He.

Figure 3: A standard polarized ^{3}He target cell. The cell consists of a spherical "pumping chamber," a cylindrical "target chamber," and a "transfer tube" connecting the two chambers. The electron beam passes through the 40 cm long target chamber as shown.

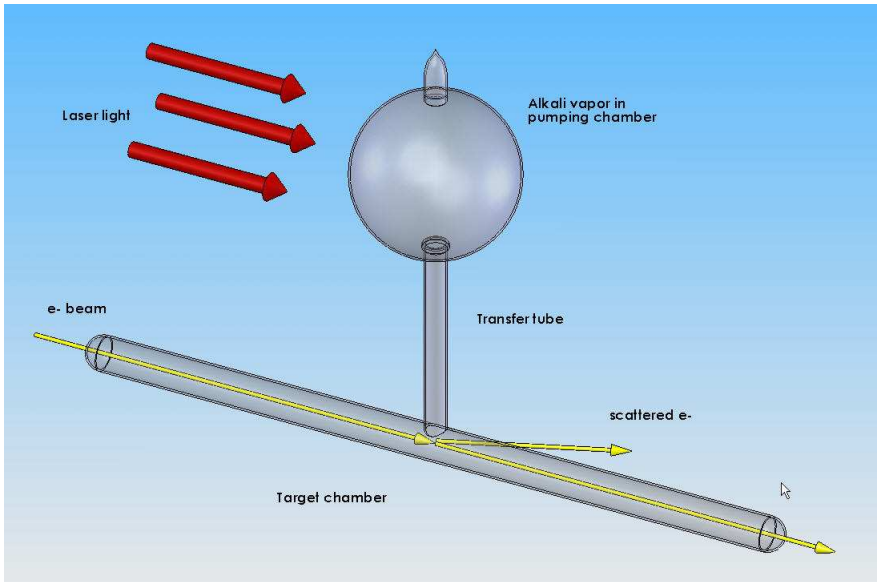

Approximately 100 Watts (total) of light from a set of 3-4 diode lasers is combined using an optical fiber coupler and directed through a series of optics to produce circularly polarized light at a wavelength of $\sim$ 795 nm. This light is used to polarize the alkali vapor through optical pumping. The polarized alkali transfers its spin to the ^{3}He nuclei through collisions.

This target has been used by seven experiments in Hall A from 1998 to 2006. During the recent GEn experiment [30] so-called 'hybrid' target cells [31] containing a mixture of potassium and rubidium were used to achieve over 55% polarization with 8 μA of beam current. During GEn target cell *Edna* was used with a beam current of 8 μA for 6 weeks without rupturing. Our studies showed that beam currents up to 10 μA could be used without much degradation in polarization and cell lifetime. Therefore we expect to achieve an average of 50% polarization for a 10 μA beam. We plan to change cells at least every three calendar weeks to avoid cell rupturing.

The target polarization can be measured using two methods: NMR and EPR (Electron-Paramagnetic Resonance). Each type of polarimetry can provide a relative 4% precision. In this document we use a polarization of 50% to estimate the expected uncertainties and beam time request.

This target continues to be a flagship facility for the Hall A program and will be relatively easy to adapt for use at 11 GeV in Halls A and C. Polarized target groups at the College of William and Mary and the University of Virginia continue to develop target cells with consistently-improving polarization. Through the combined effort of these groups and the polarized target groups and personnel at the University of Kentucky, Temple University, Duke University and Jefferson Lab this collaboration has the necessary experience and

Figure 4: Current design (side view) of the Hall A polarized target system for the series of experiments planned for 2007-08. It is expected that this target system can be used with little modification for the 11 GeV programs in Halls A and C.

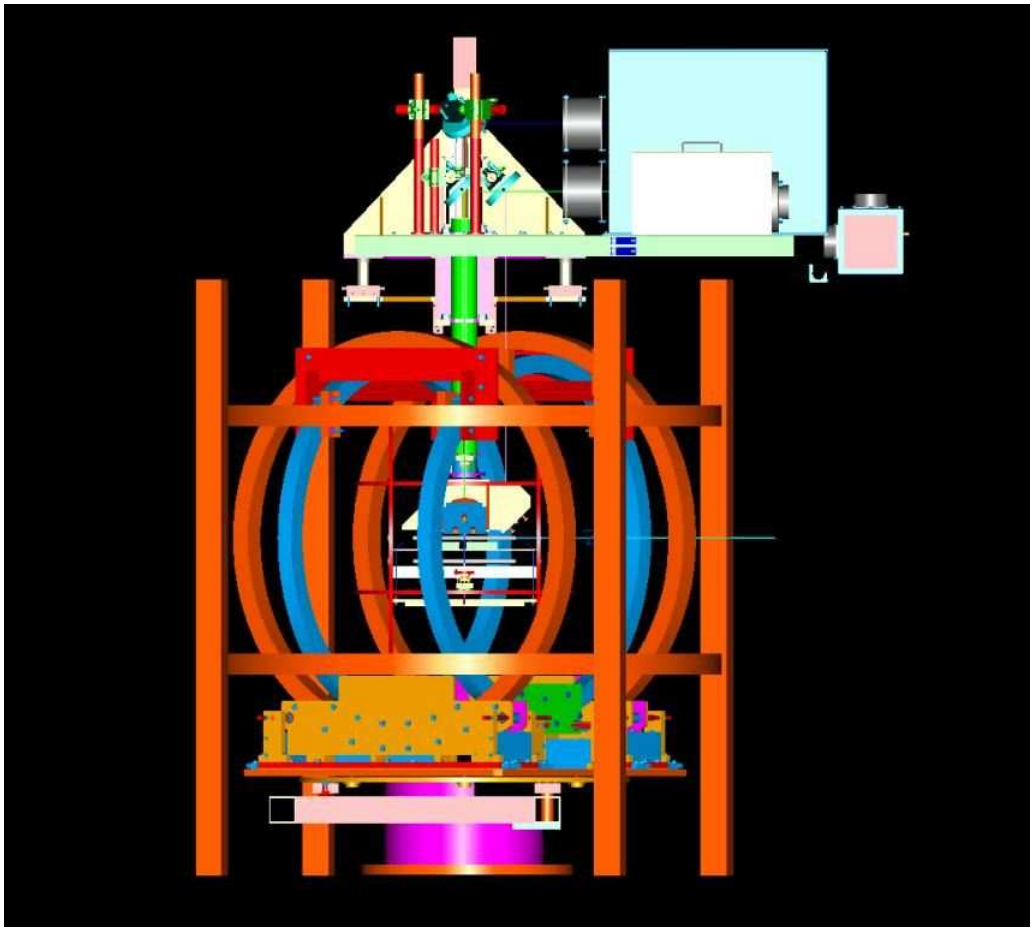

manpower for this polarized target system.

4.4 The Spectrometers setup

We plan to use the Bigbite spectrometer in Hall A to take the bulk of the data, and one HRS spectrometer, the left arm, to perform cross section measurements , cross checks on asymmetry measurements and calibrations. Both will be located at 30° with respect to the incident beam line.

4.4.1 The BigBite spectrometer

BigBite is a non-focusing large momentum and angular acceptance spectrometer that was originally designed and built for use at the internal target facility of the AmPS ring at NIKHEF [32, 33]. The spectrometer consists of a single dipole magnet (maximum magnetic

field 1.2 Tesla) and a detection system. The original detector package included two sets of multi-wire drift chambers (MWDC), a plastic scintillator and an aerogel Cerenkov detector. Since 2002, when the potential of the BigBite as an electron spectrometer for polarized target level luminosity was shown in the GEn proposal (E02-013), a long series of highly rated experiments has been approved to use this powerful device; these experiments include E04-007, E05-009, E05-015, E06-010, E06-011, and E06-014. To meet the high rate and high resolution requirements, GEn collaboration constructed a new detector package for BigBite. This detector package includes:

- Three Multi-wire Drift Chambers (MWDC) for tracking.
- A double layer lead glass calorimeter for triggering on high energy electrons and for pion rejection.
- A plane of scintillators.

The set of MWDC, calorimeter and the scintillators were successfully used during the GEn experiment, with the raw rates on the MWDC as high as 20 MHz per plane. The Gas Cerenkov counter, needed for single arm e,e' mode, is being designed now to be used for the neutron d_2 experiment (E06-014) which is scheduled to run in early 2008.

To the first order, momentum of the electrons detected by the Bigbite spectrometer is inversely proportional to the deflection angle ($\theta_{\rm def}$) through the spectrometer. This was clearly verified in the GEn experiment where the momentum determined using the simple relationship:

$$P_e = \frac{(0.306 + 0.0189 \times x_{\rm bend})}{\theta_{\rm def}} + ... \tag{15}$$

provides 1.5% level momentum resolution. As the sizes of the coefficients indicates, the correction based on x_{bend}, ($x_{bend} < 0.5$) m, the position of the track at the bend plane of the spectrometer, is at the 5% level.

For the GEn experiment, the Bigbite spectrometer was located at 52°, 1.1 m from the target while the distance between the first and the third MWDC was 0.7 m. The limiting factor on luminosity for this experiment was high rate of low energy particle hits on MWDCs. As one would naively expect, the background hit rate (and the resulting MWDC current drain) went down with the increasing beam energy. During GEn the maximum operating currents for the 1.5 GeV and 2.6 GeV beam energies were 5.5 μA and 7 μA respectively. For 3.29 GeV running, the reduced background levels allowed us to increase the current to 8 μA. A Geant simulation, normalized to GEn background rates, indicates that Bigbite spectrometer located at 30°, 1.5 m from the target and 6 GeV Beam energy (conditions for the Hall A transversity experiment which is scheduled to run in 2007) can be operated with beam currents up to 10 μA.

For the proposed measurement we plan to locate the Bigbite spectrometer at 1.55 m from the target for 8.8 GeV and 6.6 GeV beam energy running. Given the empirical evidence and simulation results, we expect to be able to run at beam currents higher than 10 μA under these conditions. However, we are taking a conservative approach in this proposal and have assumed a 10 μA beam current for the rate estimates.

The maximum momentum of the electrons detected in the GEn experiment was approximately 1.6 GeV. For the proposed experiment we plan to use BigBite to detect electrons up to 3.2 GeV. As a result, the bend angles for these electrons will be about half of those for the GEn experiment. In order to account for the smaller bend angle we will double the distance between MWDC #1 and MWDC #3 in the Bigbite detector stack from 0.7 m to 1.4 m. This will approximately double the angular resolution, resulting in a 1% level momentum resolution for the 3.2 GeV electrons, similar to the resolution achieved for 1.6 GeV electrons in the GEn experiment. This increased resolution for the proposed setup has been verified using the Bigbite Geant simulation described in the next section.

A 1% momentum resolution for the scattered electrons leads to ~ 0.007 level resolution in x_{Bj} for our highest bin at $x_{Bj} = 0.71$. With an approximate $(1 - x_{Bj})^3$ dependance of the DIS cross section in the high x_{Bj} region, the varation of cross section over one σ of x_{Bj} is roughly 7%. The bin size in x_{Bj} for this proposal is 0.05. Since this is more than 8 times the expected resolution in x_{Bj}, the 1% momentum resolution is adequate for this experiment.

4.4.2 Geant Simulation of BigBite

The package of programs for the simulation of the BigBite spectrometer characteristics was developed by V. Nelyubin [34]. The results from this simulation for the GEn configuration agreed very well with the momentum resolution and the solid angle acceptance achieved during the GEn experiment. The results of this MC study of the BigBite momentum resolution predicted for the GEn setup are shown in Fig. 5, where the momentum resolution as a function of the electron momentum for position resolutions of 0.2 mm (the resolution of the MWDC) and 1 mm are plotted. The achieved momentum resolution of ≈1-1.5% agrees very well with this simulation.

This simulation has been repeated for the conditions of the proposed experiment; electron momenta up to 3.5 GeV, Bigbite located at 1.55 m from the target with the distance between the first and the third MWDC increased to 1.4 m. Figures 6 and 7 show a top and a side view of BigBite and the other experimental components as they were described in the simulations. For this case, the expected momentum resolution is ≈1%, the expected position resolution on target along the beam is σ= 5 mm, and the expected angular resolution in both scattering planes is σ=1 mrad. The solid angle of Bigbite for different positions along the target is shown in Fig. 9. The solid angle averaged over the 30 cm target length is 50 msr for scattering angles of $30 \pm 4°$.

Additional MC studies were done to evaluate the parameters of the proposed experiment. The simulated range of Q^2 vs. x_{Bj} accepted by the Bigbite spectrometer (with a 2 GeV momentum threshold) is shown in Fig. 8.

4.4.3 The Field Clamp Configuration for Bigbite

The operation of the polarized ^{3}He target requires a uniform magnetic field; the field gradient averaged over the target volume must be below 30 mGauss/cm. During the GEn experiment, where Bigbite magnet was only 1.1 m away from the target, an iron "magnet box" was successfully used to shield the the polarized ^{3}He target from the Bigbite field. Bigbite will be placed 1.55 m away from the target for the proposed measurement. Thus in this case

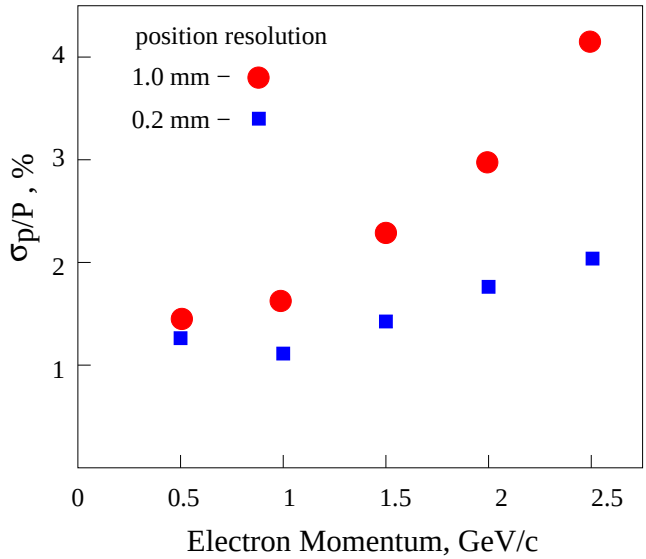

Figure 5: BigBite momentum resolution for the GEn setup as a function of the electron momentum for position resolutions of 0.2 mm (the resolution of the MWDC) and 1 mm. These are the results of a complete Monte Carlo study of the BigBite spectrometer at 52° using a gaseous helium target.

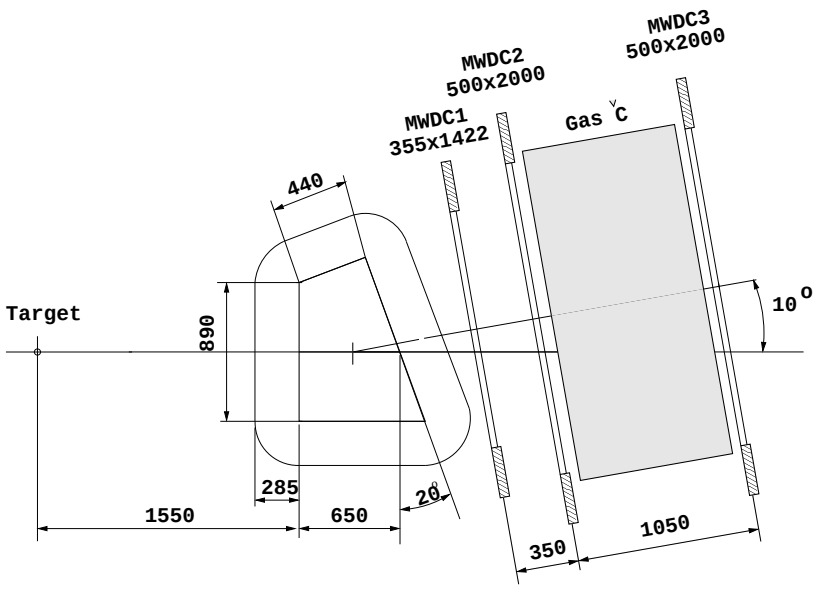

Figure 6: The side view of the experimental setup in the MC simulation. Dimensions are given in mm.

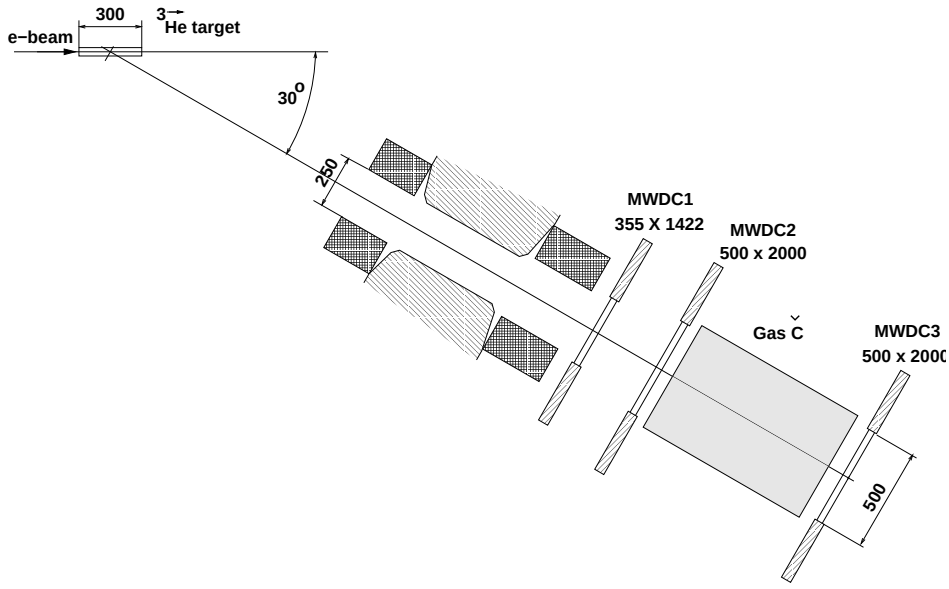

Figure 7: The top view of the experimental setup in the MC simulation. Dimensions are given in mm.

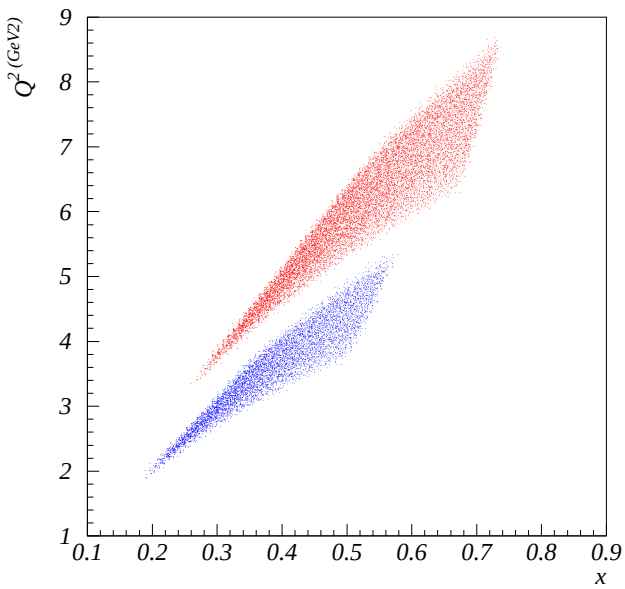

Figure 8: The Q^2 vs.x_{Bj} range for the DIS data accepted in the BigBite spectrometer for 8.8 GeV and 6.6 GeV running. A $W^2 > 4$ GeV^2 cut has been applied to select DIS data.

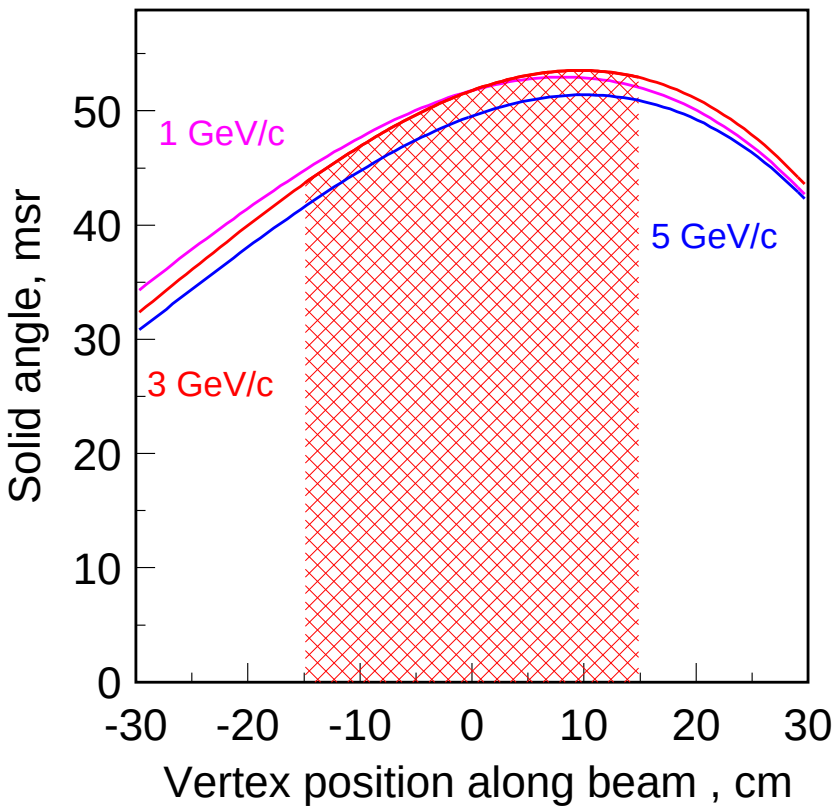

Figure 9: The MC simulation of the BigBite solid angle versus the position on target along the beam direction.

magnetic shielding of the target would be simpler than in the GEn case. Over the next few months we will study the options for reducing the stray magnetic field from Bigbite for the conditions of the proposed measurement. Figure 10 shows the first iteration of this simplified magnetic clamp configuration.

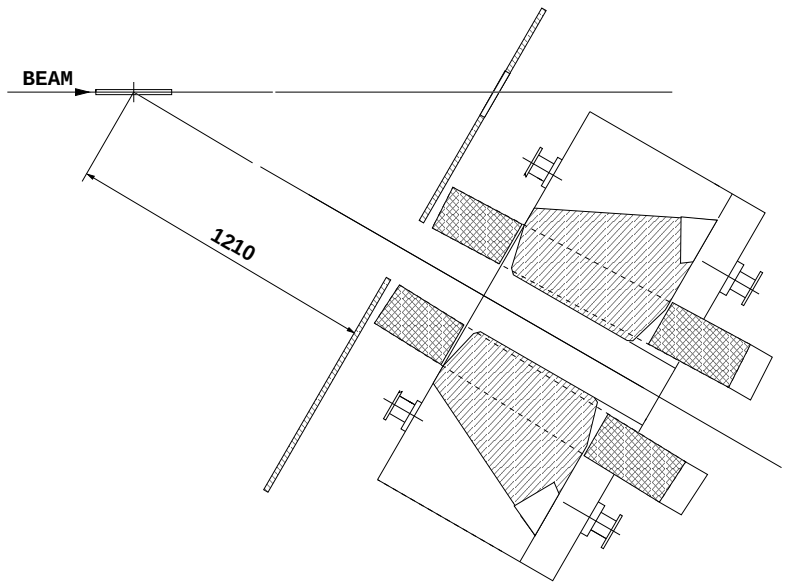

Figure 10: The concept of the field clamp configuration for the BigBite dipole.

4.4.4 BigBite Detector Package

For the proposed measurement, the BigBite detector package will consist of

- Three Multi-wire Drift Chambers (MWDC) for tracking.
- A Gas Cerenkov counter between MWDC #2 and #3 for pion rejection.
- A double layer lead glass calorimeter for triggering on high energy electrons and for pion rejection.
- A plane of scintillators.

The detector package configuration for BigBite will be similar to that of the GEn experiment with the addition of the gas Cerenkov counter that will be included for the Hall A neutron d_2 experiment. Since the proposed experiment is inclusive the addition of the Cerenkov counter for pion and proton rejection is critical.

The MWDC package was constructed at the University of Virginia funded by a NSF Major Research Instrumentation grant. The package consists of three large MWDC, each with three groups of wire-planes with wires oriented at +60° (u), -60° (v), and +90° (x). Each group consists of two wire planes. The third group of wires (x) allows unambiguous track reconstruction in a high rate environment. Furthermore, the middle chamber allows the

identification of multiple tracks at high rates. The active area of the first chamber is 35 cm $\times$ 140 cm while the active area of the second and third chambers is 50 cm $\times$ 200 cm. During the GEn experiment these MWDC performed very well in a high rate environment where the rate of raw hits on each wire-plane was as high as 20 MHz. All 2600 wires in the chambers were operational for almost continuous running during the 2.5 month long experiment with no noisy wires or dead wires. The chamber resolution obtained during online analysis was approximately 300 μm, this is expected to improve to about 200 μm after further analysis.

Figures 11 and 12 show the vertex reconstruction and momentum resolution achieved after online analysis of the GEn data.

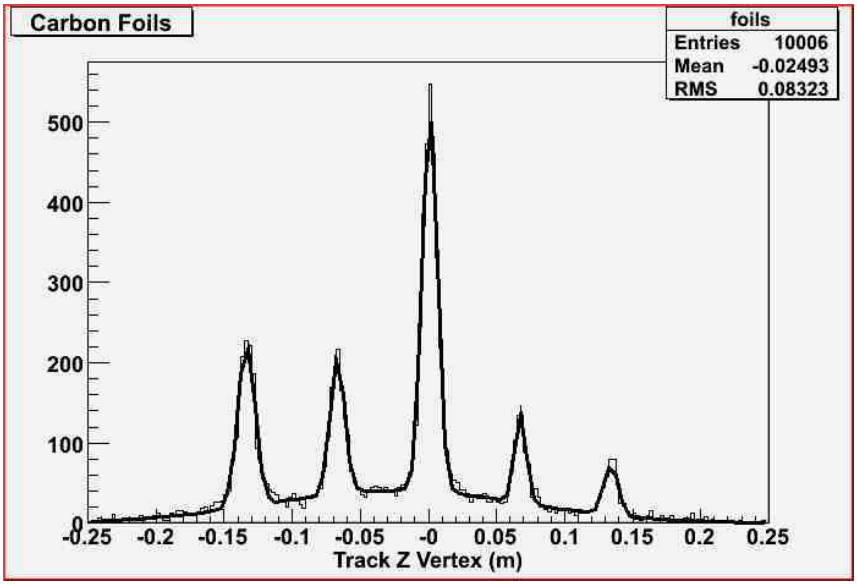

Figure 11: The vertex reconstruction of the ^{12}C foil target from the online analysis of GEn data.

The electron identification in our case is provided by the Cerenkov counter in combination with the electromagnetic calorimeter. The latter is composed by of two sub-packages. The first a preshower detector made out of blocks of TF-5 lead glass spanning an active area of 210 $\times$ 74 cm^2 with 10 cm depth (3 r.l.) along the particle direction. This is followed by a shower detector composed with total absorption blocks of TF-5 lead glass covering an area of 221 $\times$ 85 cm^2 with 34 cm depth which should contain showers with energies up to 10 GeV. The resolution of the calorimeter is about $8\%/\sqrt{E}$[GeV] leading to an expected pion rejection of 100:1 (after offline analysis).

The Cerenkov counter we plan to use for this experiment is currently being designed for the Hall A neutron d_2 experiment at 6 GeV (E06-014). It will be located in the gap between the second and third wire chambers and has the following dimensions: 200x60x60 cm^3. Cerenkov radiation emitted by relativistic particles will be collected in 10 mirrors tiled in a 5x2 arrangement at the back of the chamber. Each of those primary mirrors focuses light into a 5" PMT by way of a flat secondary mirror located toward the front of the chamber. This configuration allows the PMTs to be positioned away from the BigBite fringe field and

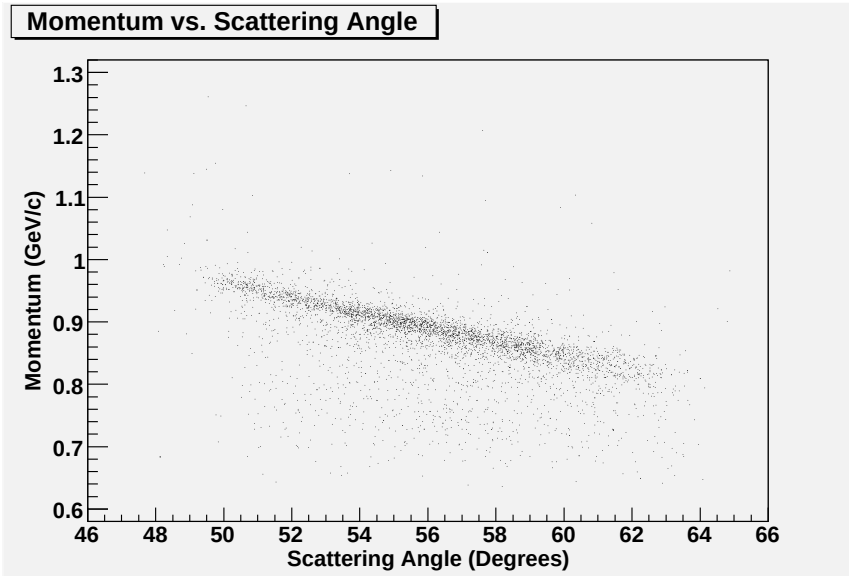

Figure 12: Reconstructed momentum vs. scattering angle showing the momentum resolution for the H(e,e'p) elastic data from GEn online analysis.

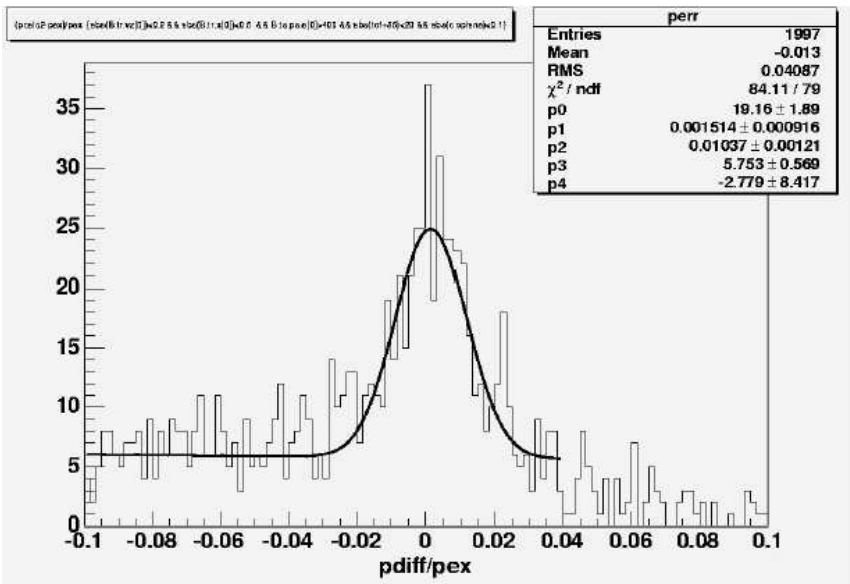

Figure 13: The difference between the reconstructed momentum for the H(e,e') elastic peak and the expected elastic momentum calculated using the scattering angle indicating the 1-1.5% level momentum resolution achieved in GEn online analysis.

provides a relatively compact design that can be installed in the existing BigBite detector frame with minimal modifications.

Our preferred choice of Cerenkov radiator is C_4F_{10} at 1 atm. This material is non-flammable, non-toxic, odorless, and does not require special handling to remain a gas at room temperature. It is currently in use in Cerenkov devices in both Hall B and Hall C at Jefferson Lab. Its index of refraction is 1.0015 giving a pion threshold of 2.5 GeV/c.

We expect a pion rejection ratio of at least 100:1 from the Cerenkov and, when coupled with cuts on the shower/pre-shower, we expect to achieve a total pion rejection of 10^4. This is adequate for the proposed measurement. The pion asymmetry will also be measured during the same experiment.

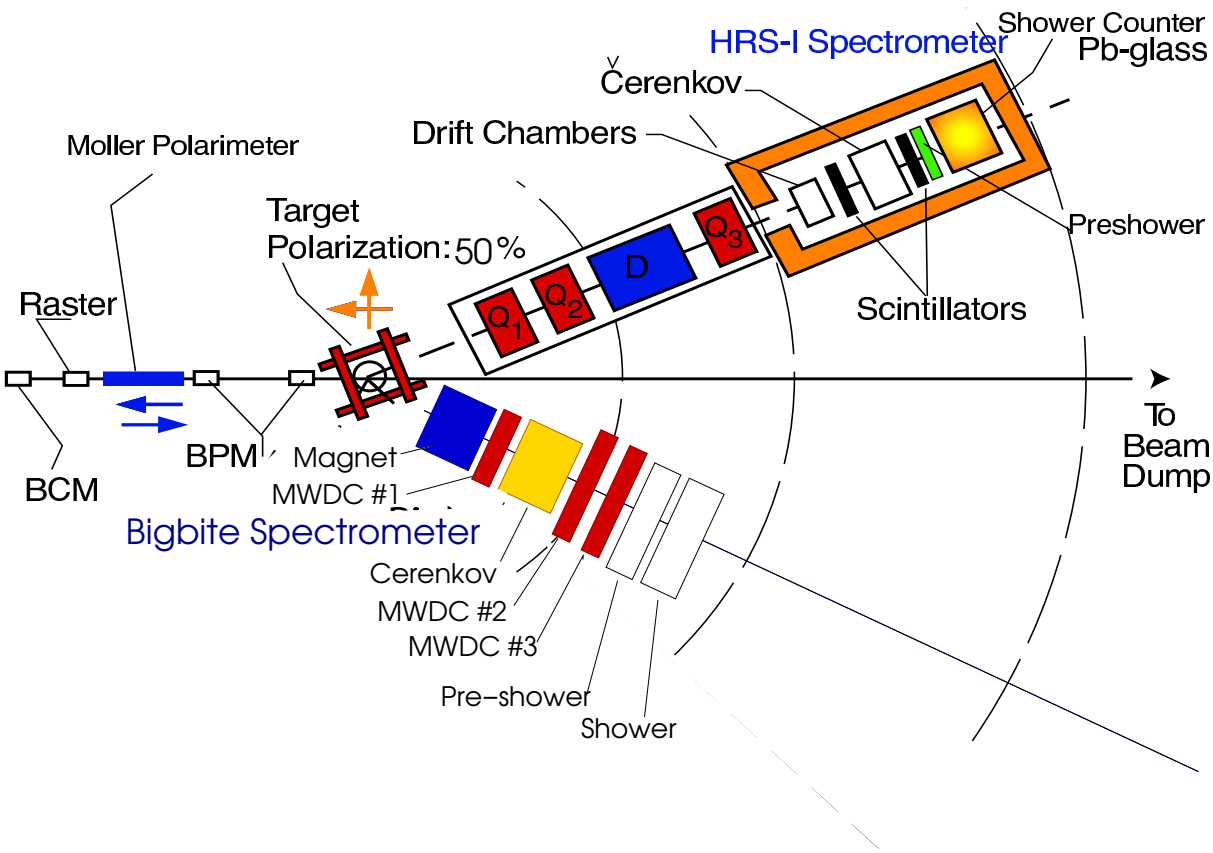

Figure 14: JLab Hall A floor setup using the Bigbite, the left HRS spectrometer and the polarized 3He target.

4.4.5 Left High Resolution Spectrometer

The Hall A left High Resolution Spectrometer (HRS) will be positioned at 30° to measure absolute cross sections in the same x_{Bj} range as the the BigBite spectrometer. We will use the left HRS with its standard detector package for electrons which consists of :

- Two vertical Drift Chambers (VDCs) for tracking.
- Threshold Gas Cerenkov counter for pion rejection.
- A set of scintillators for triggering on charged particles.
- A double layer lead glass calorimeter for additional pion rejection.

As the E99-117 analysis shows, the pion rejection factor with the Cerenkov counter and the lead glass calorimeter are better than 1×10^5 with an electron detection efficiency of 98%. This is sufficient for our worst case scenario.

Specific advantages make the HRS spectrometer a well matched tool for the proposed measurement.

- Good electron events in the spectrometer are in principle due only to electron scattering off ^{3}He nuclei since the target cell glass windows are outside the spectrometer acceptance. However, excellent target reconstruction by the HRS spectrometers allows for better background rejection.
- An excellent resolution of the spectrometers permits the measurement of elastic scattering off ^{3}He needed for an absolute calibration of the detector in order to measure absolute cross sections.

4.5 Physics background

The physics background we encounter in the DIS region is due to charged and neutral pions.

- The π^- background can be suppressed using Cerenkov and lead-glass detectors, as discussed earlier in this section.
- The decay of photo-produced π^0 creates photons which can produce (e^+,e^-) pairs. The electrons from this channel can introduce a dilution factor in the measured asymmetry. Because the yields of e^- and e^+ are the same in the pair production, one can measure the e^+ yield at the same kinematics to correct for this dilution. Due to the relatively low energy of these electrons, this dilution becomes significant only at very low x_{Bj}. Measurement of the positron production cross section during JLab E99-117 shows that it is less than 3% of the total cross section already at $x = 0.33$ and scattering angle of 35°. It was also found that the asymmetry was negligible compared to the statistical uncertainty of the measurement which was similar to this experiment. In any case we plan to measure the positron cross yields using the left HRS spectrometer and BigBite with reversed polarity from the electron detection mode.

4.6 BigBite Optics Study

In order for us to accurately determine the scattered electron's angular coordinates, momentum and the position of the scattering vertex along the target, the optics of BigBite need to be studied. Coincidence $\mathrm{H}(e, e'p)$ elastic scattering will be used to calibrate the optics. The beam will be scattered off H_2 gas filled in the reference target cell. Bigbite will be set to positive polarity detecting the proton in coincidence with a high energy electron detected in a set of lead-glass blocks.

A multi-foil carbon target will be used to calibrate the y_{target} reconstruction of the BigBite spectrometer. The calibration will be performed at first with the the Bigbite magnetic field set to zero, which will offer a check of the wire chamber geometry. The magnetic field will then be turned on to its full value for the optics calibration.

5 The Resonance region data

Although this proposal is optimized to study the DIS region, the large momentum acceptance of Bigbite provides us with the opportunity to gather two precision datasets in the resonance region at no extra cost. The resonance region A_1^n data in the high x_{Bj}, high Q^2 region covered by this proposal is of great interest:

- This data allows for a precision test of quark-hadron duality for spin structure functions in a region never been explored before. This test is made even more powerful by the fact that the resonance region data and the DIS data are obtained simultaneously using them same setup, thus canceling most systematic errors in the comparison.
- resonance region A_1^n data provides the opportunity to study spin structure functions, their Q^2 dependence and higher twist effects etc. in the very high x_{Bj} region, which is not accessible in the DIS region.

This opportunity to gather high precision resonance A_1^n data is exciting given the intriguing new results from the Hall A spin duality experiment (E01-012) [35]. Fig. **??** shows the preliminary results for the four Q^2 values of this experiment. The extraction of A_1^n from $A_1^{^3\mathrm{He}}$ has not been performed yet and the results for $A_1^{^3\mathrm{He}}$ are presented here. The qualitative behavior of A_1^n will be similar to the behavior of $A_1^{^3\mathrm{He}}$ presented here. For the two lowest average Q^2 data, it can be seen that $A_1^{^3\mathrm{He}}$ near or at the $\Delta(1232)$ peak is large and negative unlike the DIS behavior. But as the Q^2 increases, $A_1^{^3\mathrm{He}}$ crosses zero and becomes positive even in the $\Delta(1232)$ region. This is due to the rising of the non-resonant background under the resonance region. Moreover the fall off of the $\Delta(1232)$ form factors reduces the strength of the $\Delta(1232)$ as Q^2 increases. Finally, the two highest Q^2 sets of resonance data follow the same trend (see Fig **??**): this is an indication that the Q^2 dependence of A_1 has weakened as expected from the DIS data.

This may be the first indication of "x-scaling" for A_1^n in the resonance region. It would be very interesting to see whether this apparent Q^2 independence of resonance data will continue into higher values of Q^2. The two high Q^2 points for the spin duality data are at 2.6 $(\mathrm{GeV/c})^2$ and 3.6 $(\mathrm{GeV/c})^2$. The Q^2 vs. x_{Bj} coverage for the proposed measurement is

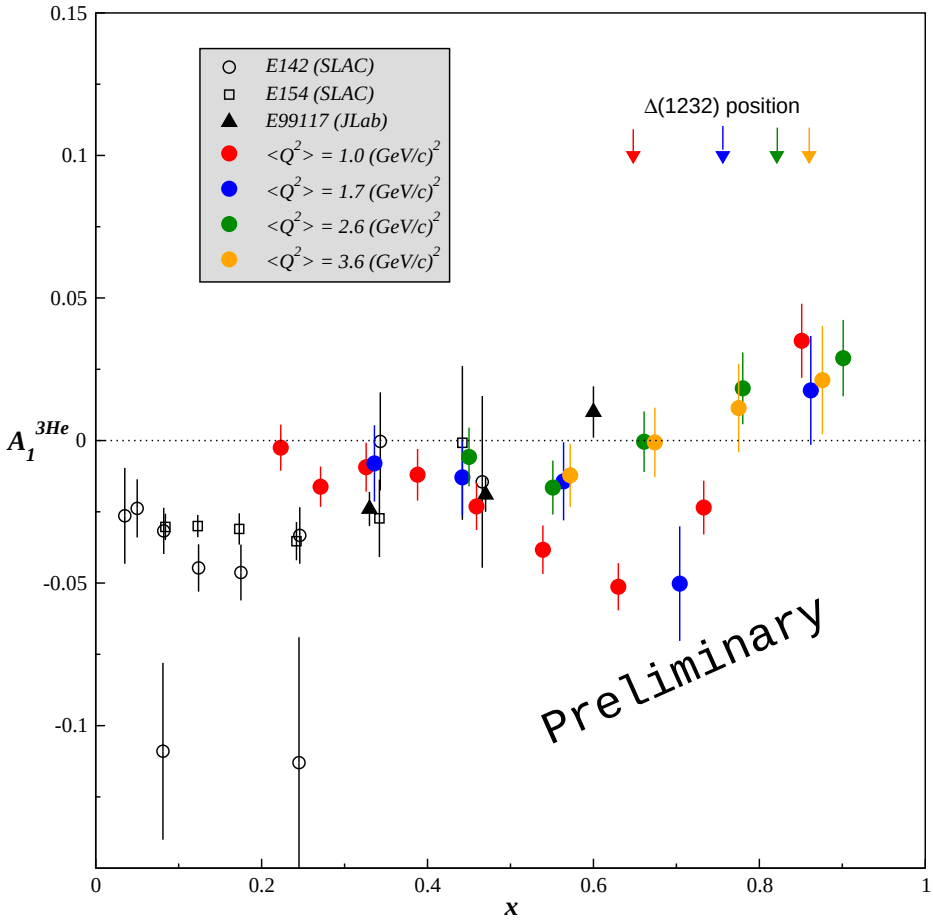

Figure 15: Results on A_1 for ^{3}He in the resonance region. Deep inelastic data from experiments at JLab (E99117 [36]).

shown in Fig. 5. The averageQ^2 values for these two settings are approximately 5 (GeV/c)^2 and 7.5 (GeV/c)^2, providing a very nice extension in Q^2 coverage to the spin duality data.

5.1 Proposed Measurement and Data Analysis

The measurement consists of collecting $^3\tilde{\mathrm{He}}(\tilde{\mathrm{e}}, \mathrm{e}')$ data at a scattering angle of 30.0° with 8.8 GeV and 6.6 GeV polarized electron beams.

The raw measured ^{3}He counting asymmetries are converted to the experimental asymme-

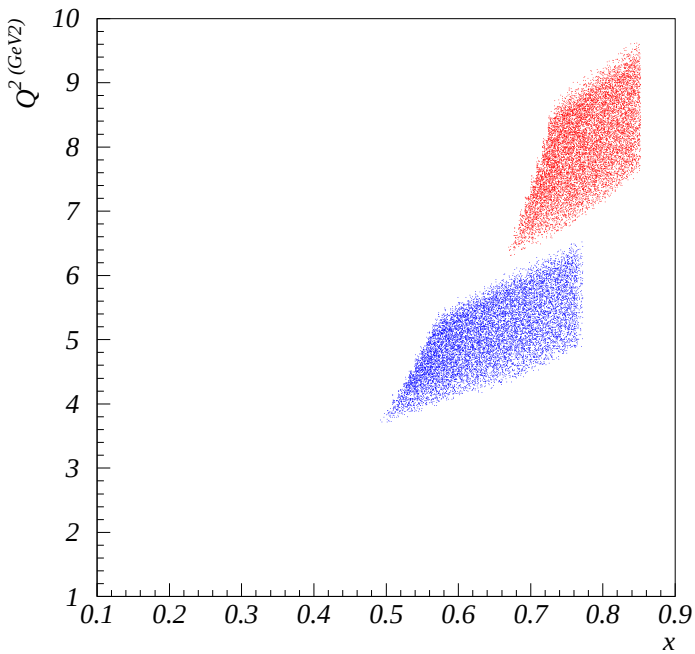

Figure 16: The Q^2 vs.x_{Bj} range for the resonance data accepted in the BigBite spectrometer for 8.8 GeV and 6.6 GeV running. A W^2 cut between 1.5 GeV^2 and 4 GeV^2 has been applied to select resonance data.

try using the relation,

$$A_{\parallel}^{^3He} = \frac{\Delta_{\parallel}}{P_b P_t f} \tag{16}$$

$$A_{\perp}^{^3He} = \frac{\Delta_{\perp}}{P_b P_t f} \tag{17}$$

$$\Delta_{\parallel} = \frac{(N^{\uparrow\downarrow} - N^{\uparrow\uparrow})}{(N^{\uparrow\downarrow} + N^{\uparrow\uparrow})} \tag{18}$$

$$\Delta_{\perp} = \frac{(N^{\downarrow\rightarrow} - N^{\uparrow\rightarrow})}{(N^{\downarrow\rightarrow} + N^{\uparrow\rightarrow})} \tag{19}$$

where $N^{\uparrow\uparrow}$ ($N^{\uparrow\downarrow}$) represents the rate of scattered electrons for each bin in W and Q^2 when the helicity of the incoming electron beam is parallel (anti-parallel) to the target spin. $N^{\downarrow\rightarrow}$ and $N^{\uparrow\rightarrow}$ correspond to the case where the target spin is perpendicular to the beam helicity. $P_b = 0.8$ and $P_t = 0.5$ are the beam and target polarizations respectively. f is the dilution factor that corresponds to the fraction of events that originated from scattering off ^{3}He. The dilution is mainly due to the small fraction of N_2 present in the target cell. The analysis of previous polarized ^{3}He experiments has indicated that the dilution factor is about 92% and it can be measured to better than 1%. Reference target runs will be used to calculate the dilution factor for the proposed experiment. The good position resolution of Bigbite and HRS-L would allow the removal of target wall events with software cuts, only a 30 cm length of the 40 cm target cell has been assumed for the rate calculations to account for this.

The radiative corrections will be applied in two steps. The external corrections will be evaluated using the Mo and Tsai prescription [37]. The internal corrections will be evaluated and corrected for by using the prescription by Kukhto and Shumeiko [38].

5.2 Systematic Uncertainties

The systematic uncertainty on A_1^n is dominated by the following terms:

1. Effective proton polarization in the ^{3}He: $P_p = -0.028 \pm 0.003$.
2. Unpolarized structure functions F_1: constructed from PDF parameterizations. We used the weighted average of MRST and CTEQ for the uncertainty on F_1^p and F_1^n [1].
3. Proton spin asymmetry A_1^P: from a fit to world g_1^p/F_1^p data, with uncertainties [36].
4. Beam and target polarizations $P_b = 0.8(1 \pm 0.5\%)$ and $P_t = 0.50(1 \pm 3\%)$.

The systematic uncertainties for the proposed measurement are smaller than or comparable to the statistical uncertainties.

5.3 Extraction of Neutron Information from ^{3}He

The neutron asymmetry A_1^n is extracted from $A_1^{3\mathrm{He}}$ as [39]

$$A_1^n = \frac{F_2^{^3\mathrm{He}}[A_1^{^3\mathrm{He}} - 2\frac{F_2^p}{F_2^{^3\mathrm{He}}} P_p A_1^p (1 - \frac{0.014}{2P_p})]}{P_n F_2^n (1 + \frac{0.056}{P_n})} , \tag{20}$$

where $P_n = 0.86^{+0.036}_{-0.02}$ and $P_p = -0.028^{+0.009}_{-0.004}$ are effective nucleon polarizations of the neutron and the proton inside ^{3}He and their current known value and full uncertainties evaluated from three N-N potential calculations [40, 39, 41]. The uncertainty on P_p dominated the systematic uncertainty for the previous A_1^n measurement. The approved Hall A experiment E05-102 [42] is aiming in studying the ^{3}He wavefunction and the uncertainties on P_n and P_p will be improved by a factor of 4 after the completion of this experiment. We therefore take $\Delta P_p = 0.003$ in our uncertainty analysis. We used a fit to world g_1^p/F_1^p data [36] to estimate the uncertainty on A_1^p needed in Eq. (20).

For the unpolarized structure functions F_2 in Eq. (20), we use the latest unpolarized PDF parameterizations [67, 68] to construct F_1 and a parameterization for R [69]. The uncertainties in F_2 are evaluated using the uncertainties of PDF's, R's, as well as the difference between the two PDF parameterizations.

[1] However, there is uncertainty in F_1^n due to nuclear effects in the deuteron, which is not included in either MRST or CTEQ analysis. This uncertainty will shift the A_1^n value for all x_{Bj} and hence is an correlated uncertainty.

5.4 Kinematics and rate estimates

Table 1 gives the beam time estimates for $E_0 = 8.8$ GeV production data and calibration running while table 3 provides the central values for scattered electron energy, Q^2 and W^2 for each x_{Bj} bin followed by the ^{3}He(e,e$'$) rate and the expected uncertainties for A_1^n for that bin. For the rate calculations we have assumed a beam current of 10 μA, and a 50 msr solid angle for Bigbite averaged over a target length of 30 cm. The resulting electron-nuclei luminosity is about $5 \times 10^{35}\text{cm}^{-2}\text{s}^{-1}$. The beam polarization was assumed to be 80% while the target polarization was assumed to be 50%. The cross sections were calculated by using the MRST [68] parametrization. The calcuated beam times were increased to account for an assumed 90% DAQ life-time and a 75% tracking efficiency.

Table 2 gives the beam time estimates for $E_0 = 6.6$ GeV production running, while table 4 provides the expected uncertainties for x_{Bj} bins for the $E_0 = 6.6$ run.

Task	Time (hours)
Production data; parallel asymmetry	275
Production data; perpendicular asymmetry	75
N2 dilution runs	10
^{3}He elastic asymmetry runs (2.2 GeV on HRS)	15
^{3}He delta asymmetry runs (2.2 GeV on HRS)	10
Bigbite optics calibration runs using H(e,e$'$p) data	50
Beam and target polarization measurements	25
Total	460

Table 1: Beam time estimates for $E_0 = 8.8$ GeV production data and calibration running.

Task	Time (hours)
Production data ; parallel asymmetry	70
Production data; perpendicular asymmetry	20
Total	90

Table 2: Beam time estimates for $E_0 = 6.6$ GeV production data.

x	E' (GeV)	Q2 (GeV^2)	W2 (GeV^2)	rate (Hz)	dA1n (Stat)	dA1n (Syst)
0.71	3.175	7.758	4.1	0.5	0.050	0.030
0.66	3.025	7.133	4.6	1.7	0.021	0.022
0.61	2.875	6.779	5.2	2.9	0.012	0.017
0.56	2.725	6.425	5.9	4.1	0.012	0.015
0.52	2.575	6.072	6.5	6.4	0.011	0.013
0.48	2.425	5.718	7.1	8.2	0.009	0.012
0.44	2.275	5.364	7.8	8.8	0.009	0.010
0.40	2.125	5.011	8.4	6.2	0.011	0.009

Table 3: Rate, Statistical uncertainty and Systematic uncertainty for the Bigbite data for each x_{Bj} bin for the $E_0 = 8.8$ GeV run.

x	E' (GeV)	Q2 (GeV^2)	W2 (GeV^2)	rate (Hz)	dA1n (Stat)	dA1n (Syst)
0.61	2.587	4.576	3.8	1.3	0.065	0.022
0.56	2.462	4.355	4.2	8.0	0.021	0.017
0.52	2.337	4.134	4.7	12.0	0.017	0.015
0.48	2.212	3.913	5.2	17.0	0.014	0.013
0.44	2.087	3.692	5.6	23.0	0.011	0.012
0.40	1.962	3.471	6.1	30.0	0.010	0.012
0.36	1.837	3.250	6.5	30.0	0.010	0.010
0.32	1.712	3.028	7.0	17.0	0.012	0.009

Table 4: Rate, Statistical uncertainty and Systematic uncertainty for the Bigbite data for each x_{Bj} bin for the $E_0 = 6.6$ GeV run.

The total measurement time as given in table 1 includes time for the following calibration tasks:

- reference cell running to determine the N_2 dilution factor.
- ^{3}He elastic asymmetry and delta asymmetry runs to cross check the product of beam and target polarization for longitudinal and transverse polarization running. These runs will be taken with one pass beam ($E_0 = 2.2$ GeV). The scattered electrons will be detected on HRS-L.
- Bigbite optics calibration runs using H(e,e$'$p) data, with Bigbite set to positive polarity detecting the proton in coincidence with a high energy electron detected in a small calorimeter.
- Beam polarization measurements with the Moller polarimeter (beam polarization will also be measured in-situ using the Compton polarimeter), and target polarization measurements using NMR and EPR methods.

Figure 17 shows the expected ^{3}He(e,e$'$) rate for each bin in x_{Bj} for 8.8 GeV running compared with the expected π^- rate. The π^- rate has been calculated using the Wiser

parametrization [70]. A 2 GeV lead-glass calorimeter threshold has been assumed. As the figure indicates, the worst case pion contamination is about 20:1. This can be easily removed by the 10^4 level combined pion rejection ratio from lead-glass calorimeter and the Cerenkov detector.

Figure 18 shows the expected uncertainties for the DIS data, compared to the results from Jefferson lab experiment 99-117, which has provided the most accurate A_1^n data to date.

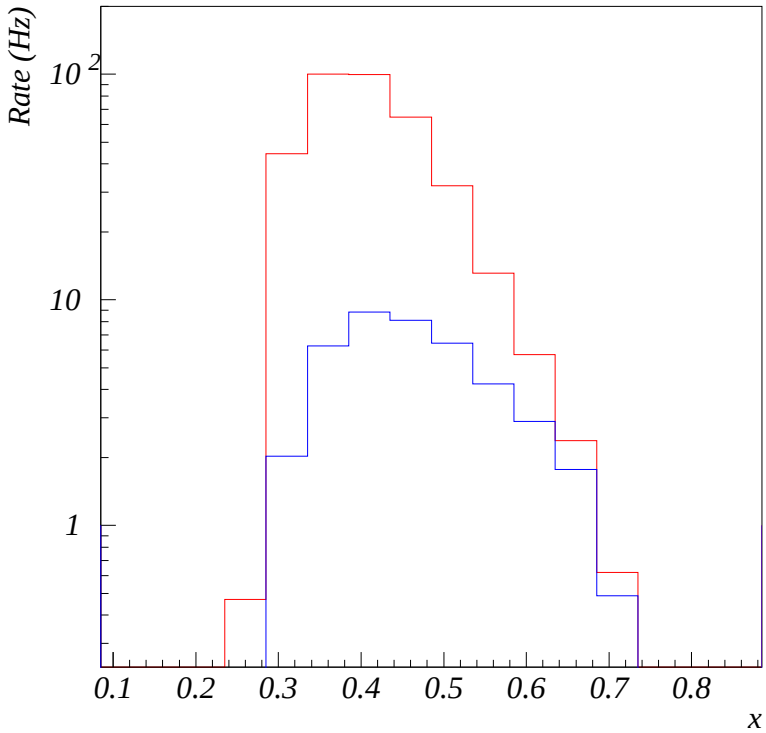

Figure 17: The projected ^{3}He(e,e$'$) (blue) and π^- (red) rates for the proposed measurement.

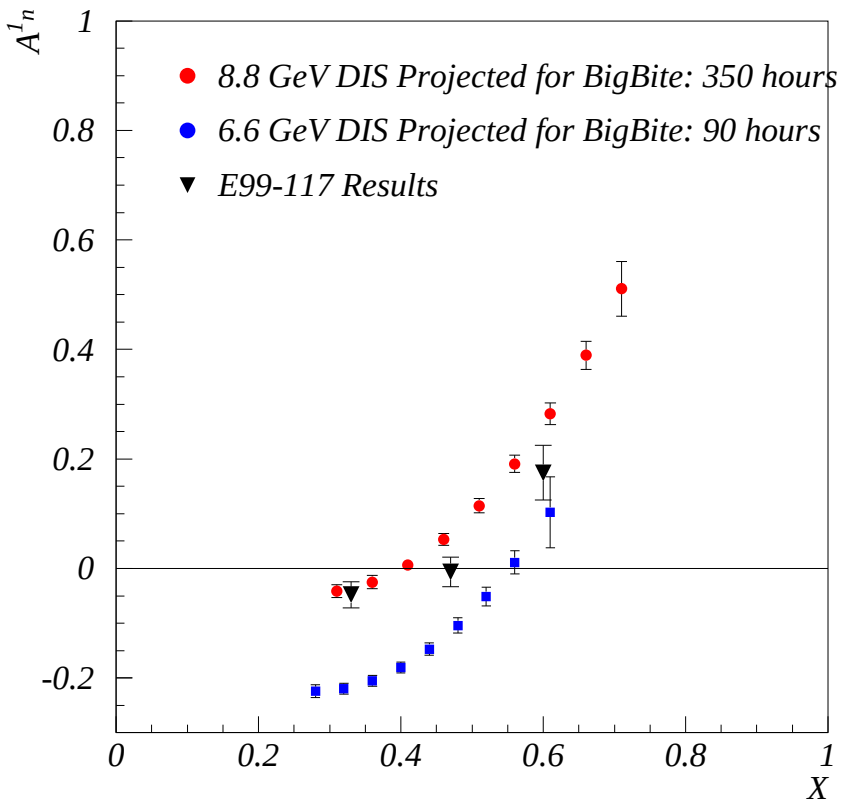

Figure 18: The projected data for the proposed measurement The solid circles show the published data from E99-117. The error bars shown are statistical only. The estimated systematic error for each point is comparable to the statistical error as shown in tables 3 and 4.

Figure 19 shows the expected uncertainties on the higher-twist contribution to $g_1^n(x, Q^2)$ if our DIS A_1^n data is included in the global analysis [?]. The uncertainties will be improved significantly in the region x¿0.3.

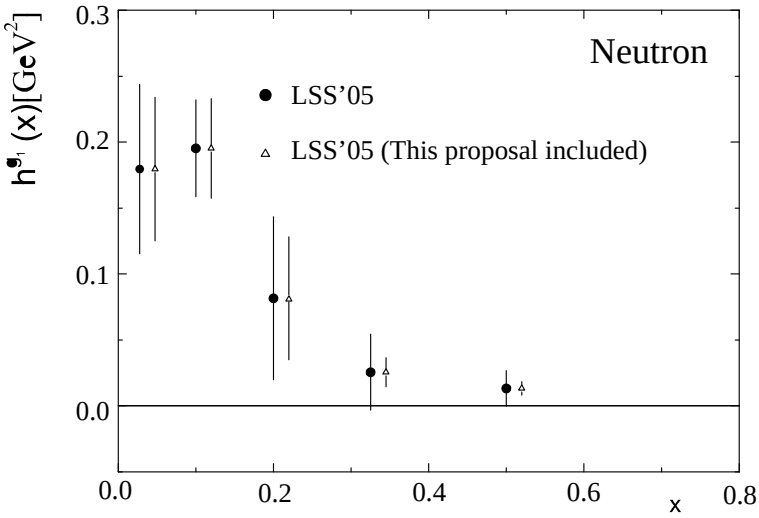

Figure 19: The projected results for the higher-twist contribution to $g_1^n(x, Q^2)$ if our A_1^n data are included in the global analysis. The LSS'05 analysis are from Ref. [71]

Fig 20 shows the expected uncertainties for the resonance region data data, which will be obtained in addition to the DIS data at no extra cost.

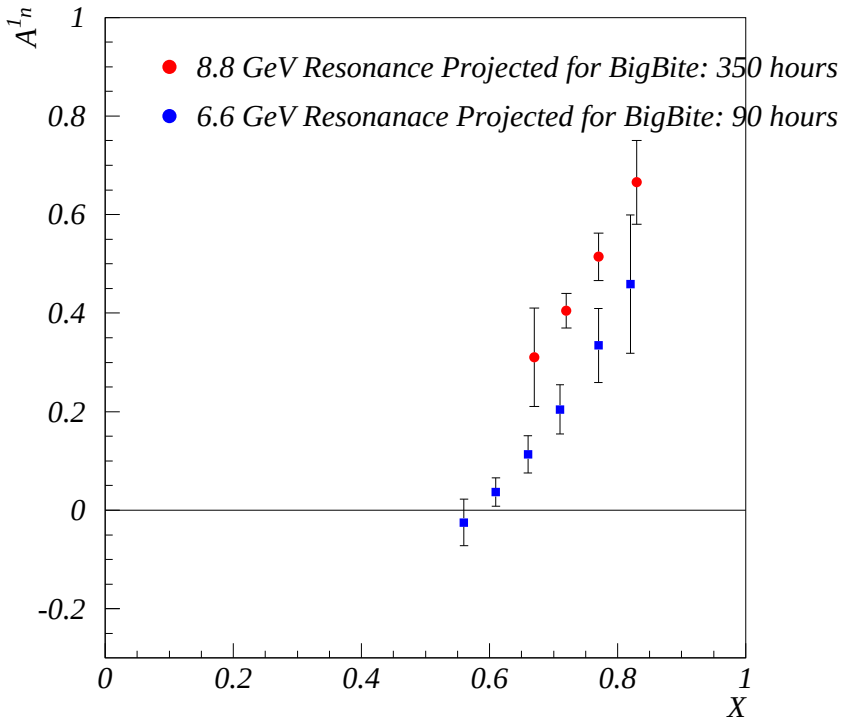

Figure 20: The projected data in the resonance region from the proposed measurement.

Fig 21 shows the expected relative statistical uncertainties for the cross section measurements on HRS-L for each x_{Bj} bin of the $E_0 = 8.8$ GeV run. The asymmetries measured on

HRS-L provides a valuable cross check of the results from Bigbite. To improve the statistical accuracy, we will re-bin the HRS A_1^n results into 4 bins covering the x_{Bj} range of Bigbite. Fig 22 shows the projected statistical uncertainties for the HRS data at 8.8 GeV.

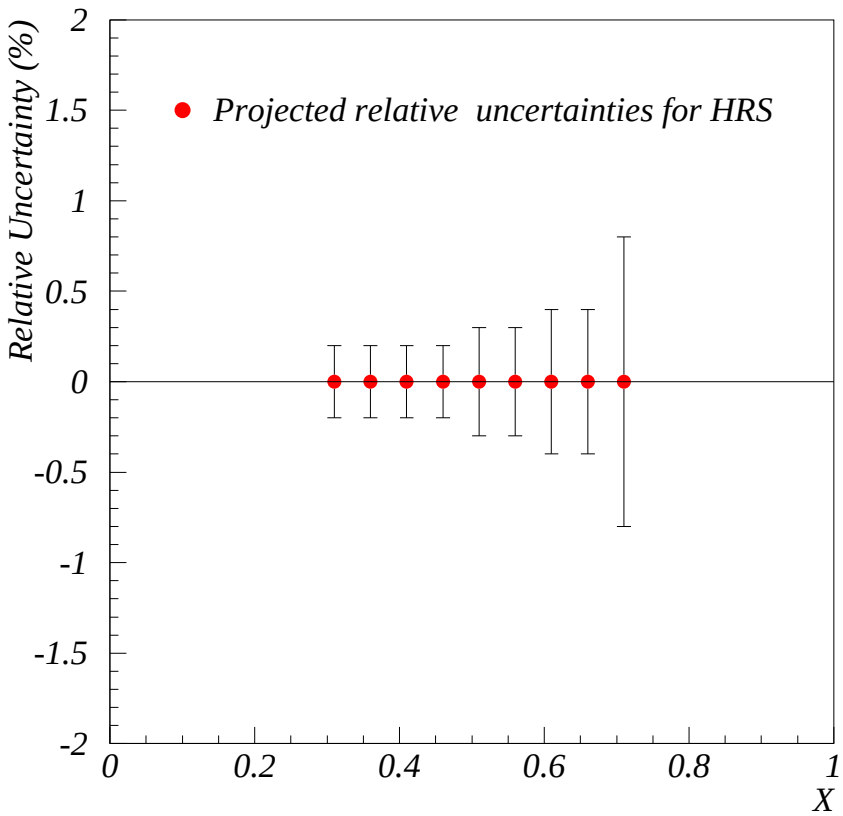

Figure 21: The projected relative statistical uncertainties for the cross section measurement using HRS-L for each data for x_{Bj} bin of the $E_0 = 8.8$ GeV run. The systematic uncertainty for cross section measurements on HRS is around 3-5%.

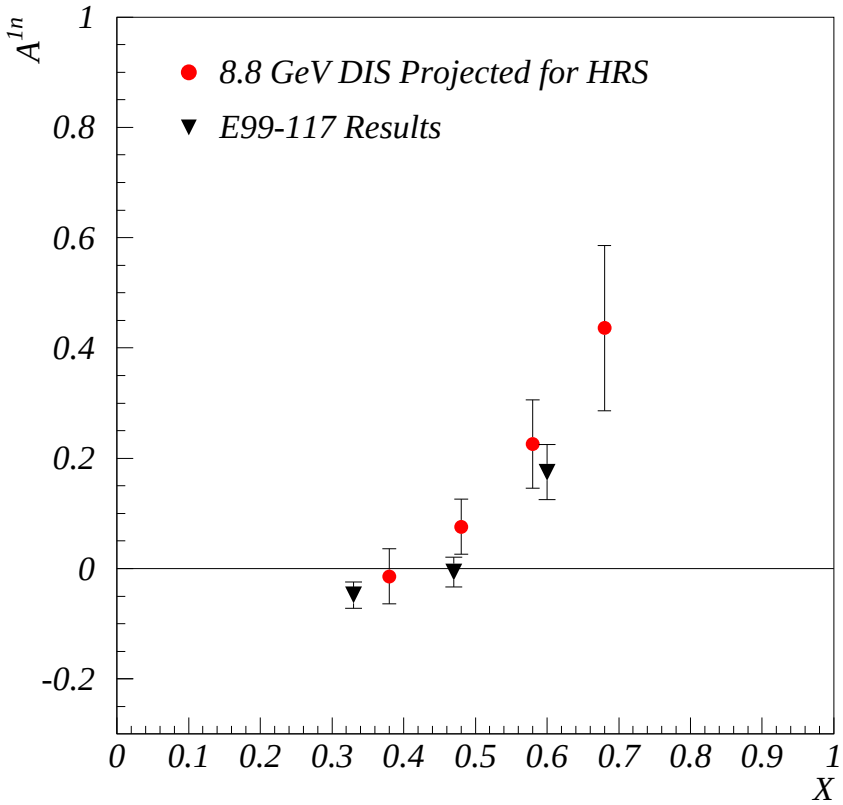

Figure 22: The projected statistical uncertainties for the A_1^n data from HRS-L (for the $E_0 = 8.8$ GeV run).

6 Summary

In summary, we are requesting 22.5 days of beam for a precision measurement of the virtual photon asymmetry A_1^n of the neutron in the DIS region up to x_{Bj}= 0.71, using 8.8 GeV and 6.6 GeV beam energies with the Bigbite spectrometer and the polarized ^{3}He target in Hall A. The results of the experiment will represent a spectacular improvement in our knowledge of A_1^n, adding greatly to our knowledge of the nuclear wave function in the valence region. The experiment will push the top of the range of x_{Bj}over which A_1^n is known from 0.60 to 0.71, a change in x_{Bj}over which A_1^n is likely to roughly double in magnitude. The experiment will greatly reduce the errors with which A_1^n is known at lower values of x_{Bj}, improving over E99-117 by more than a factor of two. And finally, the experiment will begin the important task of understanding the Q^2 dependence of A_1^n, an issue that is critical to the interpretation of the results. The data obtained, together with corresponding data on A_1^p, will permit a significantly improved understanding of the flavor-separated polarization of the parton distribution functions. And finally, the data will enable detailed comparisons with pQCD calculations, which among other things is likely to improve our understanding of the role of quark OAM in the nucleon wave function.

We have been very conservative in projecting our results. To estimate our backgrounds, we have used measured background rates from E02-013, the Hall A G_E^n experiment, and to

account for the different experimental setup, we have adjusted those measured rates with guidance from Geant. We assume an effective target length of 30 cm, a value that can easily be obtained using a 40 cm ^{3}He target cell and aggressive collimation. We accordingly have chosen a beam current of 10 μA beam because this is the current that will reproduce the singles rates in our wire chambers that we successfully tolerated during E02-013. Despite these conservative assumptions, we find a figure of merit that is roughly 2.5 higher than what can be achieved with the combination of the SHMS and the HMS combined. We believe, however, that we can substantially reduce our backgrounds, thus permitting the use of a target with a 40 cm effective length, and a 15 μA beam, which would push the improvement of the FOM to roughly 5. We have chosen, however, to base our estimates on what we believe are conservative assumptions.

The performance of the Bigbite spectrometer in the GEn experiment combined with complete Geant simulations have indicated Bigbite as an extremely powerful device for DIS experiments with the high energy CEBAF beam. Bigbite provides a large solid angle of 50 msr averaged over 30 cm of target length and an 80% momentum bite. And during GEN, Bigbite was succcessfully operated at a luminosity of around $4.5 \times 10^{36}\mathrm{cm}^{-2}\mathrm{s}^{-1}$ (this includes beam-line windows, glass, etc.). With its large acceptance in both solid angle and momentum, Bigbite is a powerful instrument for experiments with the polarized ^{3}He target and other moderate luminosity applications.

Finally, we wish to emphasize three points. Firstly, the proposed experiment will compliment nicely the kinematics being proposed for the A_1^n experiment in Hall C. Secondly, because the proposed experiment will use only existing equipment (or in the case of the Cerenkov counters equipment that is already under construction), this would make an excellent commissioning experiment. And thirdly, we wish to point out that based on event rates alone, the comparison of Bigbite's FOM with other spectrometers continues to be impressive even at x_{Bj}= 0.8 with an 11 GeV beam. As we learn more about backgrounds and issues related to particle ID, Bigbite may well be capable of even more kinematic reach than we conservatively propose here.

References

[1] X. Zheng *et al.*, Phys. Rev. Lett., **92**, 012004 (2004); Phys. Rev. C **70**, 065207 (2004).

[2] P.L. Anthony *et al.*, Phys. Rev. D **54**, 6620 (1996).

[3] K. Abe *et al.*, Phys. Rev. Lett. **79**, 26 (1997); Phys. Lett. B **405**, 180 (1997).

[4] K. Ackerstaff *et al.*, Phys. Lett. B **404**, 383 (1997).

[5] F. Close, Nucl. Phys. B **80**, 269 (1974); in *An introduction to Quarks and Partons*, p.197, Academic Press, New York (1979).

[6] N. Isgur, Phys. Rev. D **59**, 034013 (1999).

[7] C. Bourrely, J. Soffer and F. Buccella, Eur. Phys. J. C **23**, 487 (2002). C. Bourrely, J. Soffer, *priv. comm.*

[8] C. Boros and A.W. Thomas, Phys. Rev. D **60**, 074017 (1999); F.M. Steffens and A.W. Thomas, *priv. comm.*

[9] S.J. Brodsky, M. Burkardt and I. Schmidt, Nucl. Phys. B **441**, 197 (1995).

[10] E. Leader, A.V. Sidorov and D.B. Stamenov, Int. J. Mod. Phys. A **13**, 5573 (1998).

[11] E. Leader, A.V. Sidorov and D.B. Stamenov, Eur. Phys. J. C **23**, 479 (2002); E. Leader, D.B. Stamenov, *priv. comm.*

[12] H. Weigel, L. Gamberg and H. Reinhardt, Phys. Lett. B **399**, 287 (1997); Phys. Rev. D **55**, 6910 (1997); O. Schröder, H. Reinhardt and H. Weigel, Nucl. Phys. A **651**, 174 (1999).

[13] M. Wakamatsu, Phys. Rev. D **67**, 034005 (2003); *ibid.* **67**, 034006 (2003).

[14] J.D. Bjorken, Phys.Rev. **148** 1467-1478, 1966; J.D. Bjorken (SLAC) Phys.Rev.D **1** 1376-1379, 1970.

[15] J. Ashman *et al.*, Phys. Lett. B **206**, 364 (1988); J. Ashman *et al.*, Nucl. Phys. B **328**, 1 (1989).

[16] G. Morpurgo, *Physics* **2**, 95 (1965); R.H. Dalitz, in *High Energy Physics; Lectures Delivered During the 1965 Session of the Summer School of Theoretical Physics, University of Grenoble*, edited by C. De Witt and M. Jocab, Gordon and Breach, New York, 1965; and in *Proceedings of the Oxford International Conference on Elementary Particles*, Oxford, England, 1965;

[17] A. Bodek *et al.*, Phys. Rev. Lett. **30**, 1087 (1973); E.M. Riordan *et al.*, *ibid.* **33**, 561 (1974); J.S. Poucher *et al.*, *ibid.* **32**, 118 (1974).

[18] A. Benvenuti *et al.*, Phys. Lett. B **237**, 599 (1990).

[19] J.J. Aubert *et al.*, Nucl. Phys. B **293**, 740 (1987).

[20] D. Allasia *et al*, Phys. Lett. B **249**, 366 (1990); P. Amaudruz *et al.*, Phys. Rev. Lett. **66**, 2712 (1991); P. Amaudruz *et al.*, Nucl. Phys. B **371**, 3 (1992).

[21] M.R. Adams *et al*, Phys. Rev. Lett. **75**, 1466 (1995).

[22] J. Ashman *et al.*, Phys. Lett. B **206**, 364 (1988); J. Ashman *et al.*, Nucl. Phys. B **328**, 1 (1989).

[23] B. Adeva *et al.*, Phys. Rev. D **60**, 072004 (1999).

[24] K. Abe *et al.*, Phys. Rev. D **58**, 112003 (1998).

[25] F.E. Close, Phys. Lett. B **43**, 422 (1973); R. Carlitz, *ibid.* **58**, 345 (1975).

[26] A. De Rujula, H. Georgi, S.L. Glashow, Phys. Rev. D **12**, 147 (1975).

[27] N.N. Bogoliubov, Ann. Inst. Henri Poincaré **8**, 163 (1968); F.E. Close, Nucl. Phys. B **80**, 269 (1974); A. LeYaouanc *et al.*, Phys. Rev. D **9**, 2636 (1974); **15**, 844 (1977); A. Chodos, R.L. Jaffe, K. Johnson, and C.B. Thorn, *ibid.* **10**, 2599 (1974); M.J. Ruiz, *ibid.* **12**, 2922 (1975); C. Hayne and N. Isgur, Phys. Rev. D **25**, 1944 (1982). Z. Dziembowski, C.J. Martoff and P. Zyla, Phys. Rev. D **50**, 5613 (1994). B.-Q. Ma, Phys. Lett. B **375**, 320 (1996).

[28] S. Nanda and D. Lhuillier, Conceptual Design for Hall A Compton Polarimetry Upgrade http://www.jlab.org/∼nanda/compton/doc/compton_upgrade.pdf

[29] J. Alcorn *et al.*, Nucl. Inst. Meth. A **522** (2004) 294.

[30] G. Cates, N. Liyanage and B. Wojtsekhowski, Jefferson Lab E02-013.

[31] E. Babcock *et al.*, Phys. Rev. Lett. **91** (2003) 123003.

[32] D. J. J. de Lange *et al.*, Nucl. Instr. and Meth. **A 406**, 182 (1998).

[33] D. J. J. de Lange *et al.*, Nucl. Instr. and Meth. **A 412**, 254 (1998).

[34] V. Nelyubin, private communication.

[35] S. Choi, J. P. Chen, and N. Liyanage, Jefferson Lab E01-012.

[36] X. Zheng *et al.*, Phys. Rev. C **70**, 065207 (2004).

[37] L. W. Mo and Y. S. Tsai, Rev. Mod. Phys. **41**, 205 (1969).

[38] T. V. Kukhto and N. M. Shumeiko, Nucl. Phys. **B219** 412 (1983); I. V. Akushevich and N. M. Shumeiko, Nucl. Part. Phys. **20** 513 (1994).

[39] F. Bissey *et al.*, Phys. Rev. C **65**, 064317 (2002).

[40] C. Ciofi degli Atti *et al.*, Phys. Rev. C **48**, R968 (1993).

[41] A. Nogga, Ph.D. thesis, Ruhr-Universität Bochum, 2001.

[42] S. Gilad, D. Higinbotham, W. Korsch, B. Norum, S. Sirca*, JLab E05-102, Measurements of Ax and Az Asymmetries in the Quasi-elastic 3He(e,e'd) Reaction, expected to run in late 2007-early 2008.

[43] G.D. Cates, J.-P. Chen, Z.-E. Meziani and X. Zheng, A new proposal to PAC-30: Measurement of Neutron Spin Asymmetry A_1^n in the Valence Quark Region Using an 11 GeV Beam and a Polarized ^{3}He Target in Hall C.

[44] M.J. Alguard *et al.*, Phys. Rev. Lett. **41**, 70 (1978); G. Baum *et al.*, Phys. Rev. Lett. **51**, 1135 (1983).

[45] B.W. Filippone and X. Ji, Adv. Nucl. Phys. **26**, 1 (2001); X. Ji, Phys. Rev. Lett. **78**, 610 (1997); R.L. Jaffe and A. Manohar, Nucl. Phys. **B337**, 509 (1990).

[46] R.P. Feynman, Phys. Rev. Lett. **23**, 1415 (1969).

[47] A.W. Thomas and W. Weise, *The Structure of the Nucleon*, p.78 and p.100, p.105-106, Wiley-Vch, Germany (2001).

[48] Z. Dziembowski, C.J. Martoff and P. Zyla, Phys. Rev. D**50**, 5613 (1994).

[49] G.R. Farrar and D.R. Jackson, Phys. Rev. Lett. **35**, 1416 (1975).

[50] G.R. Farrar, Phys. Lett. **B70**, 346 (1977).

[51] B.-Q. Ma, Phys. Lett. **B375**, 320 (1996).

[52] D. Abbott *et al.*, Phys. Rev. Lett. **84**, 5053 (2000).

[53] K. Wijesooriya *et al.*, Phys. Rev. C **66**, 034614 (2002).

[54] M.K. Jones *et al.*, Phys. Rev. Lett. **84**, 1398 (2000).

[55] O. Gayou *et al.*, Phys. Rev. Lett. **88**, 092301 (2002).

[56] G.P. Lepage and S.J. Brodsky, Phys. Rev. D **22**, 2157 (1981).

[57] G.A. Miller and M.R. Frank, Phys. Rev. C **65**, 065205 (2002);

[58] R.V. Buniy, P. Jain and J.P. Ralston, AIP Conf. Proc. **549**, 302 (2000).

[59] A.V. Belitsky, X. Ji and Feng Yuan, Phys. Rev. Lett. **91**, 092003 (2003).

[60] X. Ji, J.-P. Ma and F. Yuan, Nucl. Phys. B **652**, 383 (2003).

[61] S.J. Brodsky, M. Burkardt, I. Schmidt, Nucl. Phys. **B441**, 197 (1995).

[62] E. Leader, A.V. Sidorov, D.B. Stamenov, Int. J. Mod. Phys. **A13**, 5573 (1998).

[63] N.I. Kochelev, Phys. Rev. D **57**, 5539 (1998).

[64] E.D. Bloom and F.J. Gilman, Phys. Rev. Lett. **16**, 1140 (1970); Phys. Rev. D **4**, 2901 (1971);

[65] F.E. Close and W. Melnitchouk, Phys. Rev. C **68**, 035210 (2003); *priv. comm.*

[66] M.V. Romalis, Ph.D. thesis, Princeton University, 1997

[67] J. Pumplin *et al.*, J. High Energy Phys. **7**, 012 (2002).

[68] A.D. Martin, R.G. Roberts, W.J. Stirling and R.S. Thorne, Eur. Phys. J. C **23**, 73 (2002).

[69] K. Abe *et al.*, Phys. Lett. B **452**, 194 (1999).

[70] D. E. Wiser, *Ph.D. thesis*, Univ. of Wisconsin, (1977);

[71] E. Leader, A.V. Sidorov, D.B. Stamenov, *Phys. Rev.* **D73**, 034023 (2006). hep-ph/0512114

[72] M. Anselmino, A. Efremov, E. Leader, *Phys. Rep.* **261**, 1 (1995).